

CTH-NT-321

THESIS FOR THE DEGREE OF DOCTOR OF PHILOSOPHY

# Neutron monitoring based on the higher order statistics of fission chamber signals

ZSOLT ELTER



Division of Subatomic and Plasma Physics  
Department of Physics  
S-412 96 Göteborg, Sweden 2016

Neutron monitoring based on the higher order statistics of fission chamber signals  
ZSOLT ELTER  
ISBN 978-91-7597-460-6

©Zsolt Elter, 2016

Doktorsavhandling vid Chalmers tekniska högskola  
Ny serie nr 4141  
ISSN 0346-718X

Division of Subatomic and Plasma Physics  
Department of Physics  
Chalmers University of Technology  
S-412 96 Göteborg  
Sweden  
Telephone +46 (0)31 772 1000

Cover: "Kandinsky lost in a fission chamber" – Various simulated heavy ion trajectories in a fission chamber and related pulse shapes illustrated in a minimalist plot.

Chalmers Reproservice  
Göteborg, Sweden 2016

Neutron monitoring based on the higher order statistics of fission chamber signals  
ZSOLT ELTER

Division of Subatomic and Plasma Physics

Department of Physics

Chalmers University of Technology

## **ABSTRACT**

The work in this thesis corresponds to the safety aspect of Generation IV nuclear systems. One of the safety aspects concerns the enhancement of the performance of the in-vessel on-line core monitoring with neutron flux measurements. It was concluded earlier that fission chambers are the best candidate to provide in-vessel measurements in sodium cooled fast reactors.

This thesis focuses on the performance of signal processing methods in order to unfold the count rate of fission chambers. The main goal is to investigate the possible application of processing methods based on the higher order statistics of the signal in order to provide accurate count rate estimation over a wide range both for stationary and transient signals. The work also consists of the study of self-monitoring capabilities in order to detect fission chamber malfunctions at an early stage. The investigation is based on analytic assessments, on simulation of fission chamber responses and signals, and on experimental application of processing methods.

The thesis covers five main studies. The first part presents the theoretical description of fission chamber signals. The second part investigates the performance of the traditionally applied methods (pulse and Campbell mode) through simulations. It is shown that these methods are not capable to cover the whole count rate range of the chamber. Therefore, the third part studies the possible application of methods based on higher order statistics of the signal through simulations and experiments. It is shown that these methods can provide accurate estimations over a wide count rate range. The fourth part covers the theoretical background of self-monitoring capabilities based on the spectral properties of the signal. Finally, the fifth part presents the implementation of the methods in a real-time neutron monitoring system based on a System on a Chip, which embeds a field-programmable gate array.

By the methods elaborated in this thesis, a faster, more effective and more accurate monitoring of the reactor power is possible than with the methods used so far, even when the normal operating state is changing.

*Keywords:* Neutron flux monitoring, Fission chamber, Filtered Poisson process, Experiment, Simulation, High order, Campbell mode



## Appended papers

This thesis is an introduction to and a summary of the work published in the following papers

### PAPER I

L. Pál, I. Pázsit, and Zs. Elter. “Comments on the Stochastic Characteristics of Fission Chamber Signals”. In: *Nuclear Instruments and Methods in Physics Research, Section A: Accelerators, Spectrometers, Detectors and Associated Equipment* 763 (2014), pp. 44–52

*The first author carried out the analytic work, and wrote the manuscript. The second author was involved in the derivations and the writing of the manuscript. The third author was involved in the verification of derivations and writing of the manuscript.*

### PAPER II

Zs. Elter, I. Pázsit, and C. Jammes. “Remark on the applicability of Campbelling techniques for transient signals”. In: *Nuclear Instruments and Methods in Physics Research, Section A: Accelerators, Spectrometers, Detectors, and Associated Equipment* 813 (2016), pp. 10–12

*The first author carried out the analytic work, performed the simulations, and wrote the manuscript. The second author was involved in the evaluation of results and the technical aspects of the manuscript. The third author was involved in the proof reading.*

### PAPER III

Zs. Elter, C. Jammes, I. Pázsit, L. Pál, and P. Filliatre. “Performance investigation of the pulse and Campbelling modes of a fission chamber using a Poisson pulse train simulation code”. In: *Nuclear Instruments and Methods in Physics Research Section A: Accelerators, Spectrometers, Detectors and Associated Equipment* 774 (2015), pp. 60–67

*The first author performed all simulations, parts of the programming needed, the analysis and wrote the manuscript. The second author was involved in the programming and the technical aspects of the manuscript. The third, fourth and fifth authors were involved in the proof reading and outline of the manuscript.*

### PAPER IV

Zs. Elter, M. Bakkali, C. Jammes, and I. Pázsit. “Performance of Higher Order Campbell methods, Part I: review and numerical convergence study”. In: *Nuclear Instruments and Methods in Physics Research Section A: Accelerators, Spectrometers, Detectors and Associated Equipment* 821 (2016), pp. 66–72

*The first author performed all simulations, the main part of the analysis and wrote the manuscript. The second author was involved in the analysis. The third author was involved in the technical aspects of the manuscript. The fourth author was involved in the proof reading and outline of the manuscript.*

#### PAPER V

Zs. Elter, G. de Izarra, P. Filliatre, C. Jammes, and I. Pázsit. "Performance of Higher Order Campbell methods, Part II: calibration and experimental application". In: *Nuclear Instruments and Methods in Physics Research, Section A: Accelerators, Spectrometers, Detectors, and Associated Equipment* 835 (2016), pp. 86–93

*The first author performed all the experiments and simulations, the post-processing, the main part of the analysis and wrote the manuscript. The second author was involved in the experiments and the technical aspects of the manuscript. The third author was involved in the simulations and the technical aspects of the manuscript. The fourth and fifth authors were involved in the proof reading and outline of the manuscript.*

#### PAPER VI

Zs. Elter, P. Filliatre, G. de Izarra, I. Pázsit, and C. Jammes. "Self-monitoring fission chamber: theoretical groundwork". In: *PHYSOR - International Conference on the Physics of Reactors, (Peer-reviewed)*. Idaho Falls, USA: American Nuclear Society, May 2016

*The first author performed all simulations, the programming needed, the main part of the analysis and wrote the manuscript. The second and third authors were involved in the analysis and the technical aspects of the manuscript. The fourth and fifth authors were involved in the proof reading and outline of the manuscript.*

#### PAPER VII

G. de Izarra, Zs. Elter, and C. Jammes. "Design of a higher order Campbelling mode measurement system using open source hardware". In: Submitted to *Nuclear Instruments and Methods in Physics Research, Section A: Accelerators, Spectrometers, Detectors, and Associated Equipment* (2016)

*The first author performed the implementations, the programming needed, the experiments, the main part of the analysis and wrote the manuscript. The second author was involved in the experiments, the analysis, the writing and the technical aspects of the manuscript. The third author was involved in the proof reading and outline of the manuscript.*

## **Related work not included in this thesis**

Zs. Elter. *pyFC: a TRIM-based fission chamber pulse shape simulator*. Tech. rep. CTH-NT-318. Chalmers University of Technology, 2015

Zs. Elter, C. Jammes, and P. Filliatre. "Simulation of stochastic processes in fission chambers". In: *International Youth Nuclear Congress*. 2014

C. Jammes et al. "Progress in the development of the neutron flux monitoring system of the French GEN-IV SFR: Simulations and experimental validations". In: *2015 4th International Conference on Advancements in Nuclear Instrumentation Measurement Methods and their Applications (ANIMMA)*. 2015, pp. 1–8

Zs. Elter. and I. Pázsit. "Energy Correlation of Prompt Fission Neutrons". In: *EPJ Web of Conferences* 111 (2016)



<b>Abstract</b>	<b>I</b>
<b>List of publications</b>	<b>III</b>
<b>Abbreviations</b>	<b>IX</b>
<b>1 Introduction</b>	<b>1</b>
1.1 Neutron monitoring . . . . .	1
1.2 Outline . . . . .	2
<b>2 Fission Chamber signal as filtered Poisson process</b>	<b>5</b>
2.1 Fission chambers . . . . .	5
2.1.1 Fissile layer . . . . .	6
2.1.2 Filling gas . . . . .	7
2.1.3 Why fission chambers in Astrid? . . . . .	8
2.2 Filtered Poisson process . . . . .	9
2.2.1 General Campbell theorem . . . . .	12
2.2.2 Campbelling for non-stationary signals . . . . .	14
2.3 Tools for the study . . . . .	15
2.3.1 pyFC . . . . .	16
2.3.2 Matlab toolbox for filtered Poisson process . . . . .	18
2.3.3 Experiment . . . . .	18
<b>3 Traditional methods: Pulse and Campbelling mode</b>	<b>21</b>
3.1 Discrete signal sample . . . . .	21
3.2 Pulse mode . . . . .	22
3.3 Campbell mode . . . . .	24
3.4 Current mode . . . . .	24
3.5 Linearity gap . . . . .	25
<b>4 Performance of Higher order Campbelling</b>	<b>27</b>
4.1 Higher order Campbelling . . . . .	28
4.1.1 Cumulant estimation . . . . .	28
4.2 Numerical studies . . . . .	29
4.2.1 Convergence . . . . .	30
4.2.2 Noise suppression . . . . .	32

4.2.3	Transient . . . . .	34
4.3	Experimental studies . . . . .	35
4.3.1	Calibration and linearity . . . . .	36
4.3.2	Transient . . . . .	39
4.4	Concluding remarks on the higher order Campbelling . . . . .	40
<b>5</b>	<b>Self-monitoring</b>	<b>41</b>
5.1	Hypothetical malfunction . . . . .	42
5.2	Impacts of pressure drop . . . . .	42
5.3	Fault indicator . . . . .	44
<b>6</b>	<b>Implementation of the measurement techniques</b>	<b>47</b>
6.1	Requirements of real-time measurements and hardware selection . . . . .	47
6.2	Implementation of HOC . . . . .	48
6.3	Implementation of the smart detector module . . . . .	50
6.4	Experimental results . . . . .	50
6.4.1	Higher order Campbelling results . . . . .	50
6.4.2	Smart detector results . . . . .	51
<b>7</b>	<b>Concluding remarks</b>	<b>55</b>
	<b>Acknowledgements</b>	<b>57</b>
	<b>References</b>	<b>59</b>
	<b>Papers I-VII</b>	<b>63</b>

## Abbreviations

<b>ADC</b>	Analog-to-Digital Converter
<b>CEA</b>	Commissariat à l'Énergie Atomique et aux Énergies Alternatives
<b>CPU</b>	Central Processing Unit
<b>DAC</b>	Digital-to-Analog Converter
<b>FPGA</b>	Field-programmable gate array
<b>FWHM</b>	Full width at half maximum
<b>HOC</b>	High Order Campbell
<b>HTFC</b>	High temperature fission chamber
<b>PSD</b>	Power spectral density
<b>SFR</b>	Sodium cooled fast reactor
<b>SoC</b>	System on a chip
<b>SPND</b>	Self-powered neutron detector
<b>TTL</b>	Transistor-Transistor Logic



# CHAPTER 1

## Introduction

The topic of this thesis is neutron monitoring, which had a major role in the safe operation of nuclear reactors since the earliest days of reactor technology. Neutron monitoring has been an active research topic at CEA (Commissariat à l'énergie atomique et aux énergies alternatives) for more than 40 years. This thesis contains the work that the author has performed during the last four years, from which 2.5 years were spent at CEA Cadarache. Neutron monitoring, based on fission chamber signal processing with the Campbell technique is treated in this thesis through numerical simulations and experiments. The main concepts of neutron monitoring and the outline of this thesis is introduced in this chapter.

### 1.1 Neutron monitoring

Our society highly relies on nuclear fission power. Although, the tendency to build new units has fallen back, many predict that nuclear fusion reactors will be built in the foreseen future. For both the fission and fusion based technologies the safety is a major issue. As far as safety is concerned, instrumentation and control plays a key role in keeping the reactor within its operational limits. Since the released power in the reactor is directly related to the neutron density, the real-time measurement of the neutrons in the system provides a sound way of estimating the released power.

Therefore, neutron monitoring has been an important part of reactor instrumentation and control since the beginning of reactor physics. In the Chicago Pile-1, Fermi was using neutron counters, in order to verify whether the neutron flux was at a safe level [1].

The heart of any neutron monitoring system is the neutron detector. Detecting neutrons is a non-trivial task, since neutrons do not ionize matter. Hence, low energy neutrons are typically detected indirectly through absorption reactions, in which a certain isotope reacts with the neutron by emitting a high energy ionized particle. Commonly used isotopes and reactions include  ${}^3\text{He}(n, p)$ ,  ${}^{10}\text{B}(n, \alpha)$  and the fission of uranium or plutonium. Applying fission isotopes is advantageous, because higher energy neutrons (having a few MeV energy) can be detected as well. The neutron detector provides an electric current, and the task of the additional

parts of the neutron monitoring system is to process this signal in order to unfold the intensity of the detected neutrons. There are several ways to process the signal, but most methods have certain limitations: they usually either work accurately at low neutron fluxes or at high neutron fluxes. Thus, the neutron monitoring system has to incorporate several independent units to cover the whole flux range of the reactor, which increases the complexity of the system [2]. Hence, it is important to investigate the possibility to apply a processing method, which can provide accurate neutron flux estimation over the whole range. By the methods elaborated in this thesis, a faster, more effective and more accurate monitoring of the reactor power is possible than with the methods used so far, even when the normal operating state is changing.

The motivation of this work was to contribute to the development of a novel neutron flux monitoring system for the French Generation IV programme. Sodium-cooled fast reactors (SFR) are among the advanced reactors selected by the Generation IV International Forum. In Europe, the development of an innovative pool-type SFR is under way, led by the French CEA and its industrial partners [3].

## 1.2 Outline

This thesis is divided into five chapters. First, Chapter 2 describes the main characteristics of fission chambers, fission chamber signals, the applied software and experimental tools, and introduces the general Campbell technique based on Paper I and Paper II. Then, Chapter 3, which is based on Paper III, reviews and studies the limitations of the traditionally applied neutron monitoring methods, the pulse and second order Campbell mode, through numerical simulations. Chapter 4 investigates the possible application of the higher order generalization of the Campbell technique in stationary and transient reactor phases. This part, based on Paper IV and Paper V, covers the numerical and experimental verification of the reliability of the higher order Campbell mode. Then, Chapter 5, which summarizes Paper VI, numerically investigates the possibility of detecting fission chamber failure based on the spectral properties of the signal. Finally, Chapter 6 presents the implementation of both the higher order Campbell mode and the failure detection method on an FPGA based board to achieve real-time monitoring. This part, based on Paper VII, reviews the challenges of the implementation to realize real-time measurements, and presents some of the experimental results obtained during the tests of the device.

One major objective during the work included in this thesis was to investigate the feasibility of applying higher order Campbell methods for real-time monitoring. Therefore, it is essential to have a proper knowledge on the accuracy of such methods, and to optimize the required measurement length in order to achieve an acceptable uncertainty, but still be able to perform as short measurements as possible. First, the random and systematic errors were assessed through

simulations, where one has an exact knowledge of the signal being processed. Second, the method was tested on experimental data, where the signal analysis was performed as post-processing, in order to verify that an accurate application is possible. Finally, the real-time feasibility of these methods had to be verified, therefore it was necessary to implement the methods on a device, which is capable to process the measured data on-line.

Most of the work in the thesis has been done by the author. However, in Paper I the application of the backward Master equation formalism, and the derivations were proposed and done by the first author of that paper, whereas in Paper VII the implementation of the Campbell and self-monitoring methods on an FPGA based system was mainly done by the first author of that paper.



## CHAPTER 2

### Fission Chamber signal as filtered Poisson process

The main focus of this thesis is on the application of fission chambers in neutron monitoring systems. The development of neutron detectors based on fissile isotopes started at the early years of the nuclear era, and has continued ever since. The research of fission chambers for neutron monitoring is still an active topic having as focus areas: to optimize detectors for high temperature applications (high temperature fission chambers, HTFC) [4], to achieve regenerative fission chamber coatings for an expanded lifetime [5], and to develop fission chamber signal processing methods for wide flux range measurements [6]. This chapter gives a short introduction on fission chambers, the theoretical background of the related signal processing methods based on Paper I and Paper II, and the tools applied in this thesis to study fission chamber signals.

## 2.1 Fission chambers

Fission chambers are nuclear detectors that are widely used to deliver online neutron flux measurements [7]. This type of detector is an ionization chamber containing fissile material in order to detect neutrons. The most common design consists of one or more electrode pairs, at least one electrode is coated with a fissile layer from a few micrograms to a few grams depending on the application. The type of the enriched fissile isotope in the fissile layer depends on the neutron energy range of interest of the neutron environment. The spacing between each anode and cathode goes from tens of microns to a few millimeters. The chamber itself is filled with pressurized gas. The body of the chamber is sealed and an insulating material insures the electrical separation between the electrodes. A schematic illustration of a simple (only one electrode coated) fission chamber is shown in Fig. 2.1. The processes leading to a current pulse after a neutron entering the chamber are the following:

- (a) When a neutron reaches the fissile coating, it is likely to induce a fission event which generates (usually) two heavily charged ions, the fission products emitted in two nearly opposite directions.
- (b) The heavy ion which is emitted out of the fissile layer ionizes the filling gas

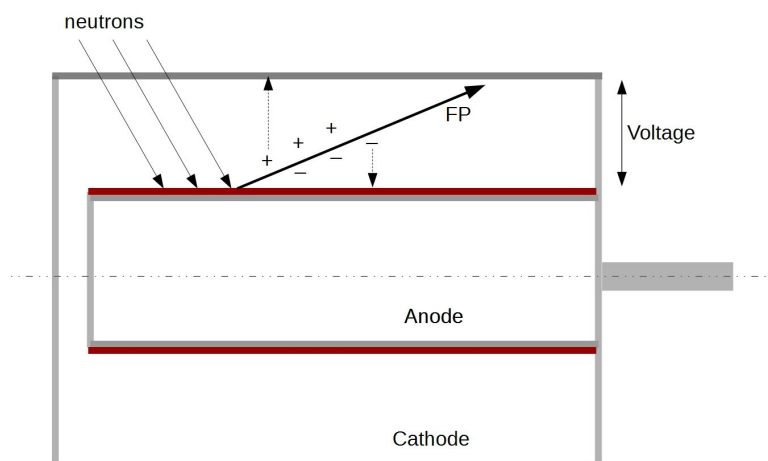


**Figure 2.1:** Schematic illustration of a fission chamber.

along its trajectory (therefore creates electron/ion pairs).

- (c) A DC-voltage of a few hundred volts is applied between the electrodes, therefore the electrons and positive ions drift across the filling gas in opposite direction towards the anode and cathode respectively.
- (d) During the drift both the electrons and the gas ions induce a current pulse (named in this thesis as electronic and ionic pulses) in the electrodes.

The DC-voltage between the electrodes must be high enough to collect all the charges, and low enough to prevent the production of secondary ionization pairs. If both conditions are fulfilled, the fission chamber operates in the so-called saturation regime, for which the neutron-induced current signal is proportional to the fission rate and nearly insensitive to the DC-voltage. In addition, one can note that the gamma particles and alpha particles that directly ionize the filling gas also generate a signal.

### 2.1.1 Fissile layer

The fission rate of the detector is given by

$$s(t) = N(t) \int \sigma_f \phi(E) dE \quad (2.1)$$

where  $N(t)$  is the number of the fissionable isotope present in the fissile deposit at time  $t$  (evolving with time),  $\sigma_f$  is the microscopic fission cross-section of the isotope and  $\phi(E)$  is the neutron spectra seen by the coating of the detector [8]. Eq. (2.1) neglects the count rate contribution of alpha particles.

The isotope of choice is determined by the application and the neutron environment. The most common deposits applied in fission chambers used for

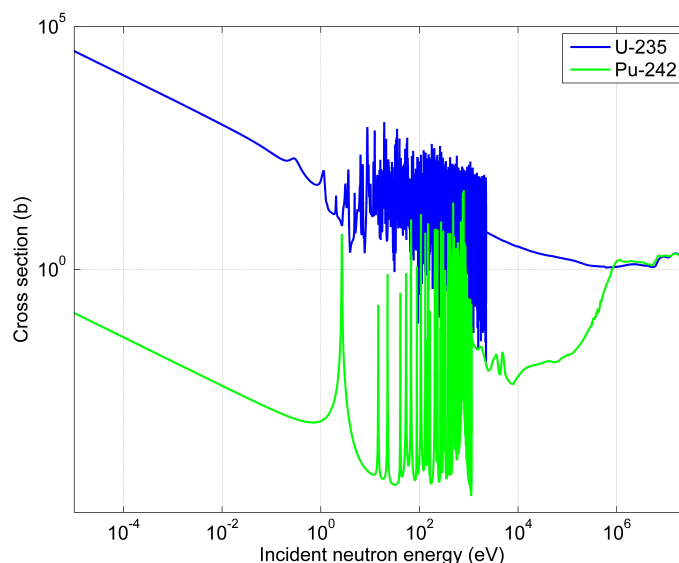


**Figure 2.2:** Microscopic fission cross sections of U-235 and Pu-242 from the JEFF 3.2 library [9].

neutron flux monitoring are made from enriched or natural uranium. Also, recently there is a novel interest in applying Pu-242 based coatings. Fig. 2.2 gives the microscopic fission cross-sections of U-235 and Pu-242. One can see that U-235 is rather sensitive to thermal neutrons. However, Pu-242 is a threshold isotope, which is sensitive to neutron energies above 1 MeV, therefore it is suitable for fast neutron measurements. Nevertheless, the fission cross-section of Pu-242 also has a significant thermal component. The joint estimation of the thermal and fast component is possible with combining the two types of fission chambers, in order to distinguish the count rate of thermal and fast neutrons [10].

As Eq. (2.1) shows, the fission rate evolves with time due to the depletion of the fissile deposit. This evolution strongly depends on the neutron fluence and spectrum (the characteristic time of the evolution can be hours or decades in different reactors). But in the applications and with the measurement times considered in this thesis (from a few ms to a few hours), the change of the fission rate due to depletion is negligible compared to the investigated count rate changes (such as control rod movement). Two possible methods are considered to overcome the problem of the time evolution: fission chambers containing regenerable fissile deposit [5, 8] and measurement systems coupled with depletion codes [11].

### 2.1.2 Filling gas

The application of monoatomic noble gas is preferred as filling gas, since the material of the electrode and the filling gas must not interact chemically and since the gamma radiation should not break up molecular bounds. The most common choice is an argon-based gas pressurized at a few bars.

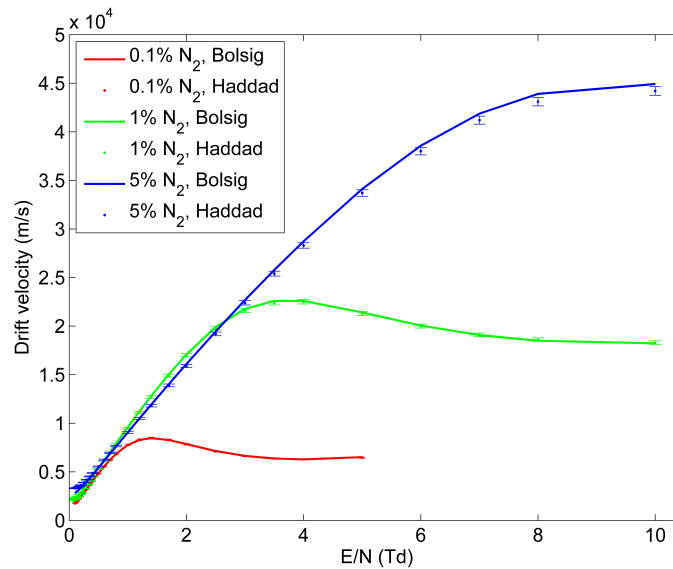


**Figure 2.3:** Electron drift velocity in Ar-N<sub>2</sub> mixtures (experimental results of Haddad [13] and BOLSIG [14] results with Biagi-v8.9 libraries [15]).

As shown later in this thesis, it is usually favorable to decrease the electron collection time and hence the width of the individual current pulses triggered by the incoming neutrons. A well-known solution to decrease the charge collection time is to add a few percents of polyatomic gas such as nitrogen [12]. Fig. 2.3 shows the drift velocity of a gas mixture as a function of the reduced electric field (which is the ratio  $E/N$ , where  $E$  is the electric field and  $N$  is the concentration of neutral particles). One can see that the electron drift velocity can be increased by a factor of four by introducing 1% of nitrogen into the mixture. However, it was observed that nitrogen molecules disappear under irradiation at high temperature of an SFR [4], therefore increasing the nitrogen content is not favorable for HTFCs.

### 2.1.3 Why fission chambers in Astrid?

Astrid will be the demonstrator prototype of the fourth generation Sodium cooled Fast Reactor technology. Generation IV systems aim to deliver advances in four broad areas: sustainability, economics, safety and reliability, and proliferation resistance. The work in this thesis corresponds to the safety aspect: an important goal is that the operation of Generation IV nuclear energy systems has to excel in safety and reliability. As far as safety is concerned, the enhancement of in-vessel on-line core monitoring is required.

The instrumentation has to fulfill the following requirements in a Generation IV fast reactor in order to detect any abnormal change in the neutron flux:

- The data acquisition system has to deliver measurements continuously and quickly.

- The measured signals have to be easy to interpret.
- The detector has to have a long lifetime (at least three operating cycles).
- The detector has to be able to provide information about both the fast and the thermal parts of the neutron spectrum.
- The measurement system has to be able to monitor the reactor over a wide power range.
- The detector has to be able to operate at high temperatures (around 600 °C).

Based on these aspects, Ref. [8] gives a detailed comparison of the performance of the most widely used neutron detectors in the existing research and power reactors: fission chambers, boron-lined counters and self-powered neutron detectors (SPND). The investigation shows that fission chambers have the longest lifetime. By using different deposits, the different parts of the spectrum can be investigated. The signal processing is relatively simple (no delayed contribution is present as in case of SPNDs), and the signal contribution of gamma radiation is relatively low. To achieve a large dynamic range one needs to combine different operating modes. The current work addresses the possibility of unifying these modes in order to further simplify the instrumentation.

Therefore, it was concluded that fission chambers are the best candidate to provide in-vessel measurements in Sodium cooled Fast Reactors.

## 2.2 Filtered Poisson process

As described earlier, a single incoming fission event in the fissile deposit triggers a detector response, a current pulse. Although, the shape of the response may vary for each event (as studied in Paper V), the impact of neglecting this variation is small when calibrating a fission chamber. Therefore, here the shape of an individual pulse is assumed to be

$$\varphi(x, t) = x \cdot f(t), \quad (2.2)$$

where  $f(t)$  is a deterministic, normalized pulse shape (defined by the actual fission chamber characteristics), and  $x$  is a random variable representing the amplitude of the pulse, characterized with an amplitude distribution  $w(x)$ .

The detector signal  $\eta(t)$  is a superposition of pulses of the form

$$\eta(t) = \sum_{k=1}^{N(t)} x_k \cdot f(t - t_k) \quad (2.3)$$

where  $t_k$  are the neutron arrival times in the detector,  $x_k$  are the random pulse amplitudes, and  $N(t)$  is the number of pulses having arrived until time  $t$ .

The fission chamber signal can be idealized as a filtered Poisson process (or shot noise). For such a stochastic process, the time interval between each pair of consecutive events has an exponential distribution with an intensity parameter. Therefore, in Eq. (2.3),  $t_k - t_{k-1}$  is assumed to be exponentially distributed with an intensity parameter (discussed later). As a consequence, the number of events, or detected pulses at time  $t$ ,  $N(t)$ , is a Poisson distributed random variable.

As described earlier, after the ionization of the filling gas by the fission fragments, both the electrons and the ions induce current pulses. This implies that the pulse function (2.2) is a composition of the electronic and ionic pulses (since by definition the ionic signal has the same count rate as the electronic signal, and the corresponding pulses arrive at the same time instant since the negative and positive charge creation is simultaneous). Although the total charge of the ions is approximately equal to the charge of the created electrons, the mobility of ions is three orders of magnitude lower in gases. Therefore, the width of ionic pulses is around three order of magnitude larger than that of the electronic pulses [16].

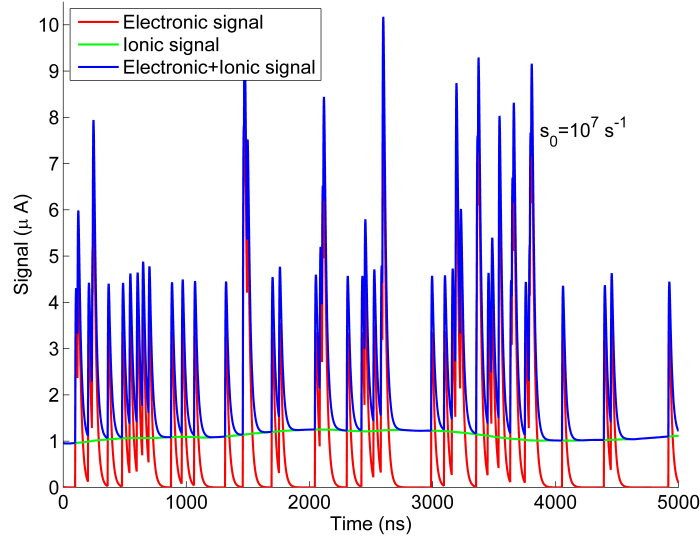


**Figure 2.4:** Illustration of a filtered Poisson process with constant intensity  $s_0 = 10^7 \text{ s}^{-1}$ .

Fig. 2.4 illustrates the filtered Poisson process as a composition of the electronic and ionic signals.

The power spectral density

$$PSD(f) = \frac{F^*[\eta(t)] \cdot F[\eta(t)]}{T_m} \quad (2.4)$$

of such an idealized filtered Poisson process (containing pulses with realistic parameters) is illustrated in Fig. 2.5 ( $F$  and  $F^*$  stand for the Fourier transformation

and the conjugate of the Fourier transformation, respectively.  $T_m$  is the measurement time). One can immediately notice that the ionic part contributes only as a low frequency noise since the ionic pulses strongly overlap already at low count rates as shown in Fig. 2.4. As such, it is often buried in the noise of the electronics and with the appropriate acquisition system it could be filtered out. Therefore, in the following analytic work, the ionic contribution is not considered. Nevertheless, the impact of it will be investigated in Chapter 4.

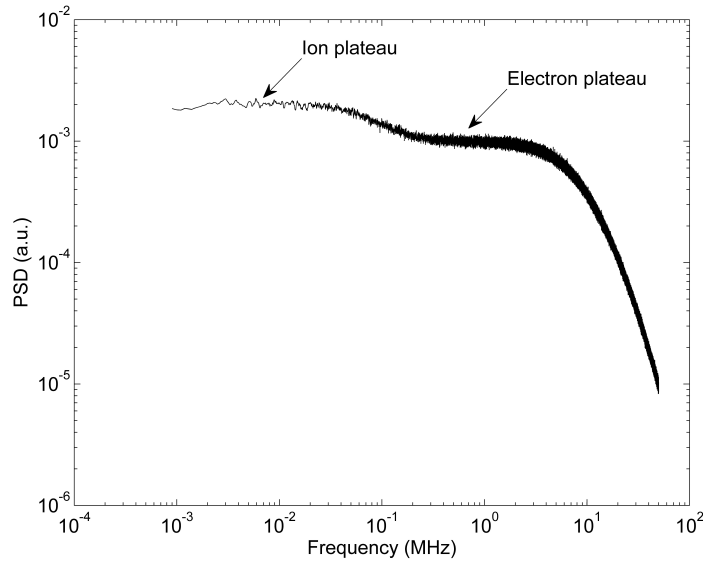


**Figure 2.5:** Illustration of the PSD of an idealised signal.

To verify the Poisson characteristics of the fission chamber signals, a measurement was performed at the MINERVE reactor (described in Sec. 2.3.3). During the measurement a fission chamber was located in the reflector of the reactor core. The time between the pulse arrivals was measured at low count rates (when the reactor already reached criticality). The probability density function of the time difference between the arrivals is shown in Fig. 2.6. The fit of an exponential distribution shows a good agreement with the empirical result (with 99% confidence). The filtered Poisson process model was accepted to describe the mathematical behavior of the fission chamber signal.

Since the fissile deposit is relatively thin, it can be assumed that the self-absorption in the layer is negligible [17]. Thus, nearly all of the heavy ions emerging from the fission event, and traveling towards the gas gap, will create a pulse. Therefore, the intensity, or count rate of the filtered Poisson process will be approximately equal to the fission rate defined in (2.1). If the count rate is time dependent, the process is inhomogeneous. If the count rate is constant in time ( $s(t) = s_0$ ), the process is homogeneous. In the following, the inhomogeneous property due to the depletion of the deposit is neglected. But the time dependence of the count rate due to the change in the neutron flux will be considered in the numerical and experimental investigations.

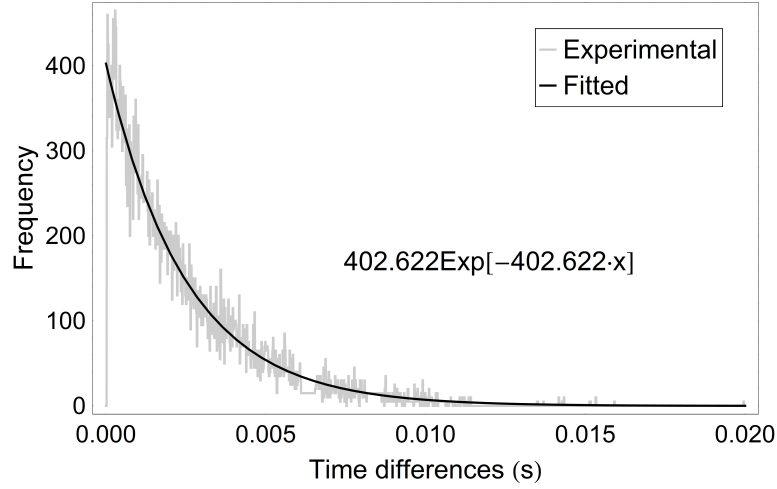


**Figure 2.6:** Verification of the Poisson nature of fission chamber signals.

## 2.2.1 General Campbell theorem

Campbell derived a linear relationship between the variance of a filtered Poisson process and its count rate [18]. It has been proposed that one can expand Campbell's theory for higher order cumulants of the signal in order to suppress the impact of unwanted minority components (such as gamma detections) [19]. The derivation of the general Campbell equations has been done previously in Refs. [20] and [21]. In this section, a recent, straightforward derivation, based on the master equation technique is summarized, which is detailed in Paper I.

In the following, the probability density function of a filtered Poisson process and the general Campbell equations are derived. The pulses in the process are considered having the shape defined in (2.2). The signal is assumed to be zero, when the measurement starts.

At the beginning, we consider that the process is an inhomogeneous Poisson-process. The probability that there are no arriving particles during the time interval  $[t_0, t]$  (where  $t_0 \leq t$ ) is given by (2.5), where  $s(t)$  is the intensity of the process (should not be mistaken for the parameter  $s$  of the Laplace transform which will be used later).

$$T(t_0, t) = \exp \left\{ - \int_{t_0}^t s(t') dt' \right\}. \quad (2.5)$$

The probability that the detector response (with shape (2.2) and amplitude distribution  $w(x)$ ) after the arrival of one single particle is not greater than  $y$  at the time  $t$  is given by the distribution function

$$H(y, t) = \int_0^\infty \Delta[y - xf(t)] w(x) dx \quad (2.6)$$

where  $\Delta(x)$  is the Heaviside step function. The probability density function can be gained by the derivation of (2.6):

$$h(y, t) = \int_0^{\infty} \delta [y - xf(t)] w(x) dx. \quad (2.7)$$

The distribution function of the sum of detector responses (the signal)  $\eta(t)$  is

$$\mathcal{P} \{ \eta(t) \leq y | \eta(t_0) = 0 \} \equiv P(y, t | 0, t_0) = \int_{-\infty}^y p(y', t | 0, t_0) dy' \quad (2.8)$$

A backward-type Chapman-Kolmogorov equation can be written for the probability density function  $p(y', t | 0, t_0)$  by summing up the probabilities of the mutually exclusive events as

$$p(y, t | 0, t_0) = T(t_0, t) \delta(y) + \int_{t_0}^t T(t_0, t') s(t') \int_0^y h(y', t - t') p(y - y', t | 0, t') dy' dt'. \quad (2.9)$$

If the Laplace-transform of the amplitude distribution  $w(x)$  is denoted as

$$\tilde{w}(s) = \int_0^{\infty} e^{-sx} w(x) dx \quad (2.10)$$

then the Laplace-transform of the probability distribution (2.7) becomes

$$\tilde{h}(s, t) = \int_0^{\infty} e^{-sy} h(y, t) dy = \int_0^{\infty} e^{-sxf(t)} w(x) dx = \tilde{w}[sf(t)] \quad (2.11)$$

With these definitions, the Laplace transform of the Chapman-Kolmogorov equation (2.9) is

$$\tilde{p}(s, t) = T(t_0, t) + \int_{t_0}^t T(t_0, t') s(t') \tilde{h}(s, t - t') \tilde{p}(s, t | 0, t') dt'. \quad (2.12)$$

where  $t_0 = 0$  and  $\tilde{p}(s, t | 0, 0) = \tilde{p}(s, t)$ . The integral equation (2.12) can be rearranged as a differential equation and solved for homogeneous case ( $s(t) = s_0$ ). The final form of the Laplace transform  $\tilde{p}(s, t)$  is then

$$\tilde{p}(s, t) = \exp \left\{ -s_0 \int_0^t [1 - \tilde{h}(s, t')] dt' \right\} = \exp \left\{ -s_0 \int_0^t [1 - \tilde{w}[sf(t)]] dt' \right\} \quad (2.13)$$

If only the stationary case ( $t \rightarrow \infty$ ) is considered, the Laplace transform reads as

$$\lim_{t \rightarrow \infty} \tilde{p}(s, t) = \tilde{p}_{st}(s) = \exp \left\{ -s_0 \int_0^{\infty} [1 - \tilde{w}[sf(t)]] dt \right\} \quad (2.14)$$

The cumulants of the distribution function are given by definition [22] as

$$\kappa_n^{(st)} = (-1)^n \frac{d^n \ln(\tilde{p}_{st}(s))}{ds^n} = (-1)^n \frac{d^n s_0 \int_0^\infty [\tilde{w}[sf(t)] - 1] dt}{ds^n} \quad (2.15)$$

which finally results in the general form of the Campbell-equation

$$\kappa_n^{(st)} = s_0 \int_{-\infty}^{+\infty} \left[ \int_0^{+\infty} (xf(t))^n w(x) dx \right] dt = s_0 \langle x^n \rangle \int_{-\infty}^{+\infty} f(t)^n dt \quad (2.16)$$

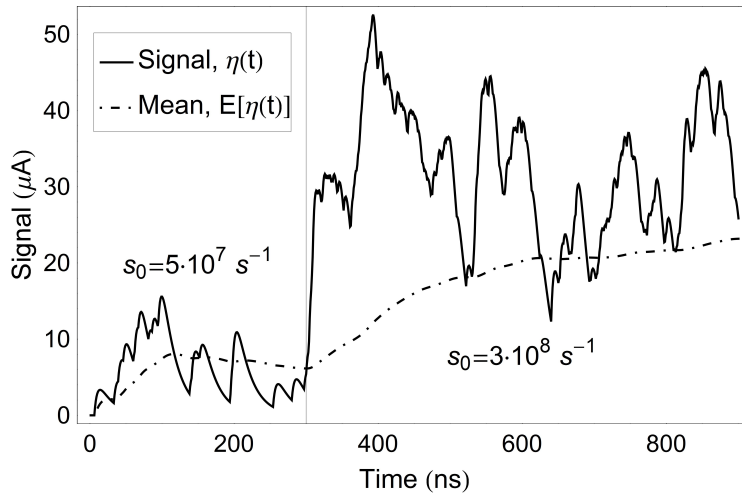
Eq. (2.16) gives a relationship between the cumulants of the signal and the pulse characteristics. In this thesis, the goal of the derivation was to reach the general Campbell-equations, but the previous derivations also provide an opportunity to determine the probability density function of the process for specified pulse shape and amplitude distribution. Further results can be found in Paper I.

## 2.2.2 Campbelling for non-stationary signals

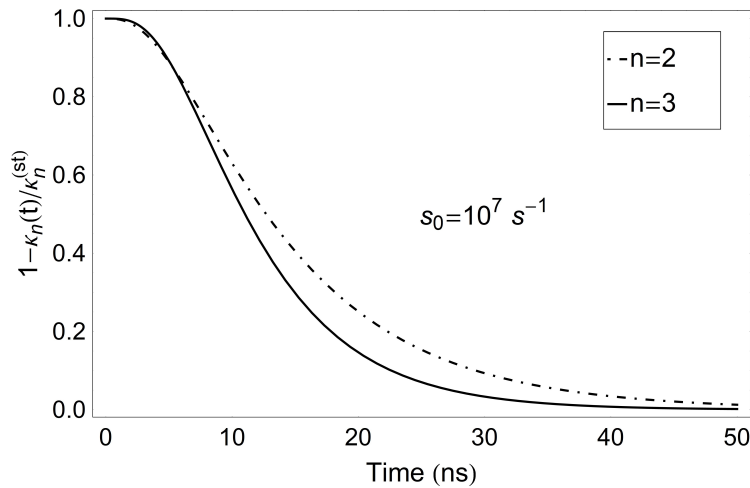
In Eq. (2.15) the stationarity of the signal was assumed. The term stationarity may be confusing for processes with a constant intensity. Stationarity means here that the time averaged cumulants of the process reach a constant value. Fig. 2.7a illustrates such behavior. The count rate of the illustrated process suffers a step change at 0 and at 300 ns. Although, the count rate becomes constant immediately after the changes, the time averaged mean of the signal needs time to reach a constant level. One should investigate how long time it takes after a step change in the flux before the stationary state is reached. To illustrate this, Eq. (2.13) was solved for a specific case: the intensity of the detection events follows a step change ( $s_0 = 0$ , when  $t < 0$  and  $s_0 = 10^7 \text{ s}^{-1}$ , when  $t \geq 0$ ), and the pulses have damped exponential shape with realistic parameters (resulting around 100 ns pulse width).

Fig. 2.7b illustrates the function  $1 - \frac{\kappa_n(t)}{\kappa_n^{(st)}}$  to give an idea about the convergence time. The results show that the values of the theoretical cumulants converge quickly to their stationary values after the step change. The convergence time can be measured in tens of ns, which is comparable with the pulse width. Neither the pulse amplitude distribution, nor the count rate have any impact on the speed of the convergence.

The derivations in the previous section become elaborate if one tries to include a time dependent count rate (i.e. consider an inhomogeneous process). Nevertheless, the results for a step change imply that in practical situations (when the change of the count rate is slower than few thousand ns), the signal can be considered as a transition of quasi-homogeneous and quasi-stationary signals, therefore no special Campbell-equation has to be derived to measure transient events. Further remarks on the stationarity can be found in Paper II, and this assumption for transient signals is investigated with simulations and experiments in Chapter 4.



(a) Illustration of non-stationarity.



(b) Time dependence of cumulants after a step change in the detection intensity.

**Figure 2.7:** Non-stationarity of homogeneous processes.

## 2.3 Tools for the study

The analytic derivations provide important insights about the characteristics of filtered Poisson processes. Nevertheless, performing the inverse Laplace-transform of the probability density function (2.13) is possible only for a few specific pulse shapes and amplitude distributions. The real shape of the detector response function, and the amplitude distribution of the chamber are rather complicated, and usually cannot be described analytically. Also, the solution of Eq. (2.12) for inhomogeneous processes becomes cumbersome. In addition, the impact of the noise of the electronics, and other unwanted signal contributors cannot be considered in the analytic derivations.

Therefore, the investigation of fission chamber signals and the performance of

various signal processing methods requires to develop numerical simulations and to perform experiments. The following section summarizes the applied numerical tools and experimental setup in order to study the fission chamber response and signal.

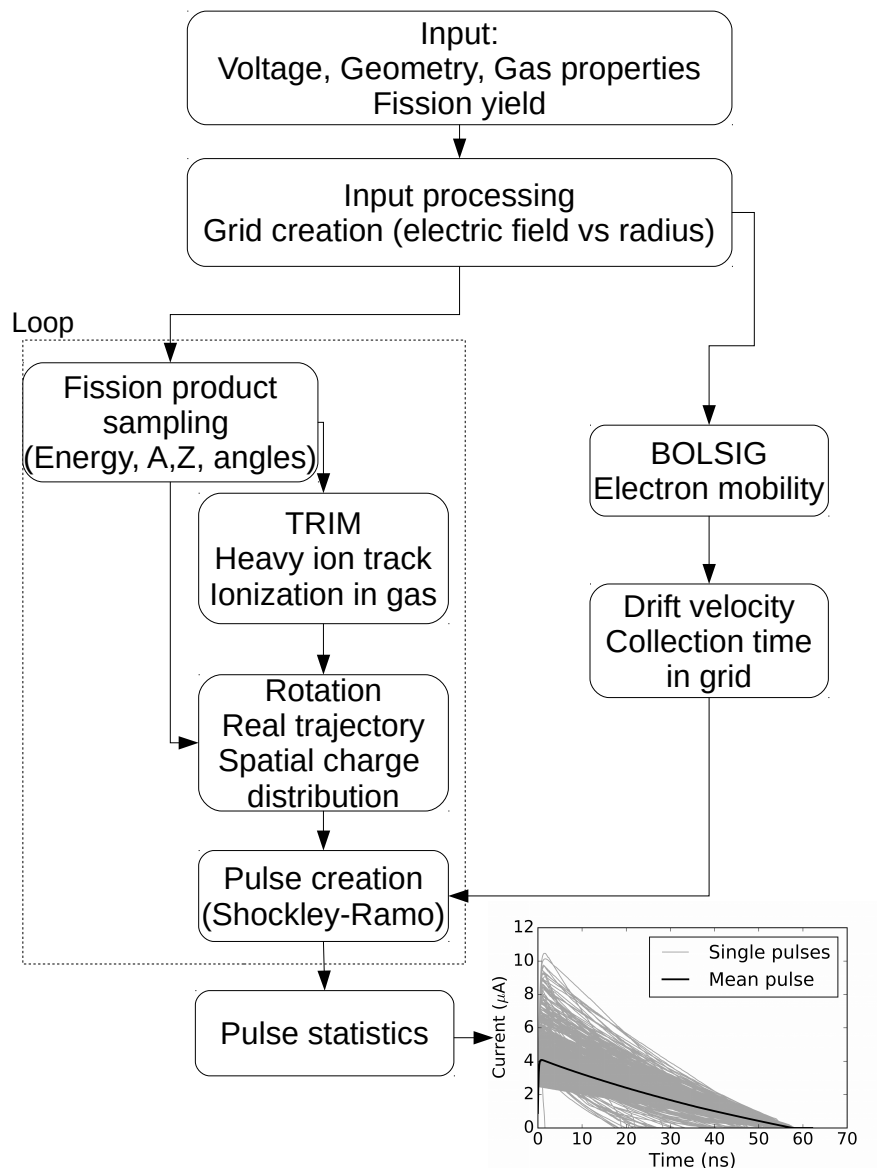
### 2.3.1 pyFC

In order to simulate the current pulse creation in fission chambers, a code suite, named pyFC (*python*-based simulation of Fission Chambers) was developed. Although similar software tools already exist (such as described in Refs. [16, 23, 24]), pyFC aims to provide a straightforward, and fast computation route in order to facilitate the study of propagation of technological uncertainties to fission chamber signals.

The working scheme of pyFC is illustrated in Fig. 2.8. The suite first samples the fission products, then the trajectories of the fission fragments in the filling gas, and the spatial distribution of the created charges along the trajectories are computed with the TRIM code [25]. TRIM (Transport of Ions in Matter) is a collection of Monte Carlo based programs which determine the stopping power and range of ions and heavy ions in matter. Since TRIM defines the target material as a 3-dimensional bulk cuboid, and in fission chambers the target material (filling gas) usually has a cylindrical shape, some geometrical rotations are performed in the suite based on the initial incident angles of the ions. The parameters of the charge collection (such as the electron mobility in the gas) is calculated with the BOLSIG software [14]. The coupling of the codes is done in Python. The collection time of the charges is calculated in a numerical grid. The current pulse creation is based on the Shockley-Ramo theorem [26]. The suite outputs the time-resolved pulses created in each event, and allows to investigate the statistics of the pulses. The details of the implemented considerations behind the code system are described in [27].

The code does not consider any recombination events and avalanches, which means that the chamber is assumed to work in the saturation regime. The space charge effects are neglected (each fission product entering the inter-electrode space ionizes the gas independently). Only the current induced by the electrons is considered, since the mobility of the ions created by the fission fragment is much lower. The original version of the code suite neglects the self-absorption of the fission fragments, but the most recent version already includes the heavy ion transport within the fissile deposit.

Multi-electrode and multi-coating chambers can be investigated with superposition, i.e. combining the results of more runs, each corresponding to one fissile coating by assuming that the inter-electrode spaces are mutually independent.

**Figure 2.8:** Flowchart of pyFC.

### 2.3.2 Matlab toolbox for filtered Poisson process

A MATLAB toolbox was implemented to simulate the fission chamber signal as a filtered Poisson process. The program generates the Poisson pulse train according to a pre-defined pulse shape, amplitude distribution and count rate. The generated signal is time-resolved like a real signal measured by an acquisition system, with a user-defined sampling frequency.

The pulse shape and the amplitude distribution can be defined as analytic functions (in order to provide comparison with theoretical results, as shown in Paper III) or may be defined by external data (e.g. from a measurement, in order to support the interpretation of measurements). The count rate may be defined as constant or as a time dependent function (in order to study transient events).

The user has the opportunity to define additional time signals, such as background noise or further Poisson trains and add these to the original pulse train. This way, the performance of signal processing methods can be investigated in the presence of unwanted signal contributors.

An important real detector-like feature of the simulation tool is the way how signals at high count rates are handled. If the order of count rate is comparable to the order of time resolution of the simulated signal, more than one pulse can appear within one time step. In this case those pulses will sum up, so the current delivered by the entirely overlapping pulses will not be lost.

The simulated signal is considered as a current signal, since in an industrial application the fission chambers are usually connected to current sensitive pre-amplifiers which can be located farther away from the core [28].

The toolbox includes a set of algorithms to estimate the count rate with various methods.

### 2.3.3 Experiment

During the work, two main experiment campaigns were done at CEA Cadarache. The first aimed to verify the applicability and the calibration of higher order Campbell methods. The second focused on the test of a real-time measurement system, which is detailed in Chapter 6.

Both experimental setups consisted of a current-sensitive fission chamber placed in the reflector zone of the MINERVE reactor [29], which is a pool type zero-power, light water reactor, operated at CEA Cadarache with a maximum power of 80 W.

In the experiments, a CFUL01 fission chamber (manufactured by Photonis) [30] was studied. The CFUL01 is a multi-electrode and multi-coating detector, which means that the chamber contains three coaxial electrodes and four fissile coatings of enriched uranium. The sensitive length of the detector is 211 mm and the outer

radius of the first electrode is 14 mm, the inner and outer radii of the cathode is 16 and 17 mm, and the inner radius of the second anode is 19 mm. Therefore the gas gap is 2 mm wide for both the inner and the outer chambers. The nominal operating voltage is 600 V (and the maximum voltage is 800 V at 20 °C, while the limit is 1300 V with no radiation). The filling gas is Argon with 4 % Nitrogen at 250 kPa (at room temperature). The fissile deposit consists of  $U_3O_8$ , with the U-235 content enriched to 90 % with a surface density of 1.32 mg/cm<sup>2</sup>. The thickness of the deposit is around 1.5 μm. The advantage of using multi-coating detectors is to increase the fissile mass in the chamber without increasing the surface mass and therefore the self-absorption of the deposit [17].

The fission chamber was connected to a fast broadband current pre-amplifier with a high immunity, 25 m long cable. The pre-amplifier acts as a high-pass filter in order to remove the DC part of the signal. It exhibits a sensitivity of  $3.08 \cdot 10^{-5}$  A/V and its gain is  $\pm 0.5$  dB in the 5 kHz - 50 MHz frequency band. During the first measurement campaign, the output signal of the pre-amplifier was digitized at a high sampling frequency (1 GHz) during a large time span with an advanced digital oscilloscope (Agilent Infiniium). The collected signals were post-processed with MATLAB. During the second measurement campaign the output signal was processed in real-time with a prototype, FPGA based measurement device (having 125 MHz sampling frequency), developed at CEA Cadarache.



## CHAPTER 3

### Traditional methods: Pulse and Campbelling mode

The generated current signal at the electrodes of the fission chamber is collected, amplified and processed. The main goal of the fission chamber signal processing is to estimate the count rate, i.e. the intensity  $s_0$  of the signal, since this value is related directly to the neutron flux. Increasing intensity causes pile-ups of the pulses in the signal, whereas the electronic noise and the background level of the gamma and alpha radiation also pose challenges, thus the estimation of the count rate becomes a non-trivial task.

Depending on the count rate, the pulse shape and the signal sampling, the chamber is traditionally operated in three different modes: the pulse mode at low power levels, the Campbelling mode at medium and high power levels and the current mode at high power levels. All modes require a separate electronic acquisition system. Therefore, a traditional instrumentation based on fission chambers is a complex system which includes various processing electronics. This chapter introduces the traditional fission chamber modes, and investigates the performance of them through simulations. This chapter mainly summarizes Paper III. Similar results can be found in the literature [2, 31], nevertheless Paper III provides an extensive sensitivity study of the linearity of the traditional methods.

### 3.1 Discrete signal sample

In the previous chapter the fission chamber signal was considered as a continuous-time signal. In measurements (and in numerical simulations), after digitizing the signal, only a finite and discrete-time signal slice is available as shown in Fig. 3.1. The sampling rate is defined by the measurement device (by the Analog-to-Digital converter) or by the user in a simulation. Later on the following notation will be used to describe the sampled current quantities:

$$X_i = \eta(t_i) \quad \text{where } i \in [1, N] \quad (3.1)$$

where  $N$  is the size of the sample (defined by the length of the measurement and the sampling rate).

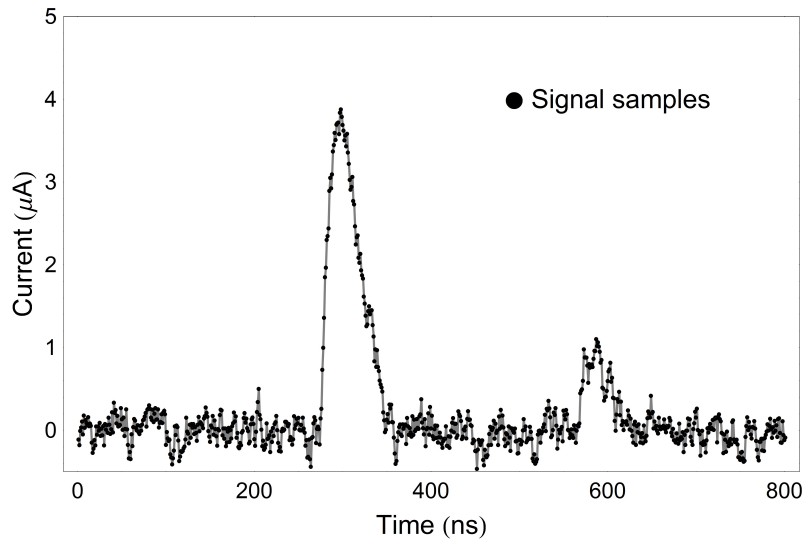


Figure 3.1: Sampled signal.

## 3.2 Pulse mode

The simplest way to estimate the intensity of the signal is through counting the pulses separately. The limitation of the separation between pulses is determined by the pulse width and the pulse intensity, as well as by the detector electronics.

In practice the counting process is achieved by a transistor-transistor logic (TTL). A discrimination level is set and when the chamber signal jumps from below to above this level, the electronics trigger a logic signal. The logical responses are counted in order to estimate the pulse count. This logic response has a certain time width and during this time the following jumps above the discrimination level are neglected. The application of such a counting system on a measured signal slice is illustrated in Fig. 3.2. The width of the TTL signal acts as a non-paralyzable dead-time (while the logical signal is on, the system will not count other pulses). The discrimination level has a paralyzable dead-time effect (meaning that if the signal stays above the level, then the electronics does not trigger more logic responses). Such a behavior can be observed in Fig. 3.2 (where a relatively high count rate was chosen in order to highlight the dead-time effect). The actual behavior depends on the TTL width, the pulse width, the pulse amplitude distribution and the discrimination level. In theory it is possible to perform dead-time corrections up to a certain extent [32].

Defining the optimal discrimination level is non-trivial. In case the pulse amplitudes are randomly distributed and the lower amplitudes are comparable with the amplitude of the noise, such a pulse counting method fails to estimate the pulse count properly. Fig. 3.3 shows the counted pulses in a 10 ms long measurement depending on the discrimination level: in case the discrimination level is too low, the noise triggers spurious counts; in case the level is too high, the method does not count low amplitude pulses. A possible option is to set the

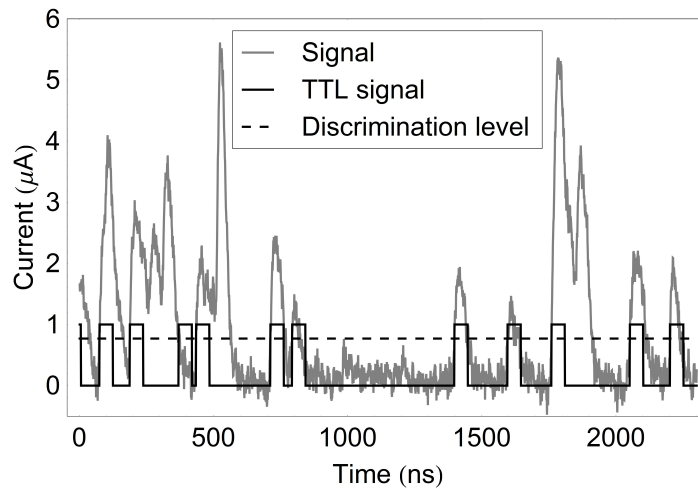


**Figure 3.2:** Illustration of a generated TTL signal.

discrimination level at the inflexion point of the curve (which is named integral bias curve in Ref. [33]).

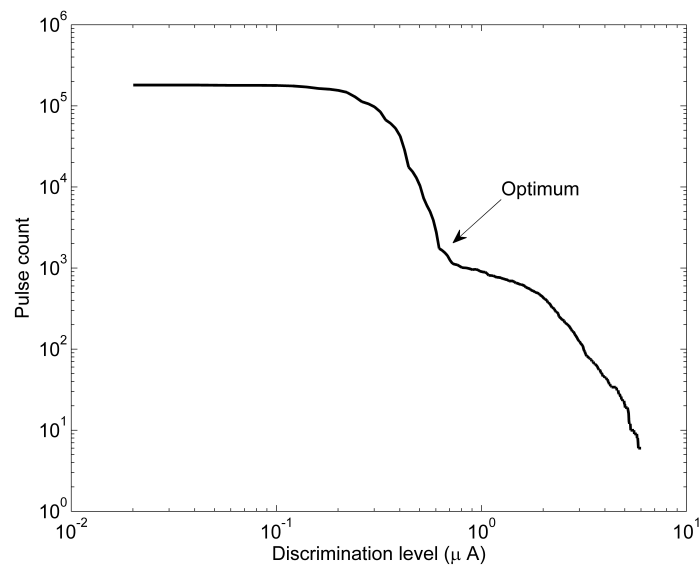


**Figure 3.3:** Estimated pulse count vs discrimination level.

In the simulations of the pulse mode included in the following sections, both dead-time phenomena inherently occur (the non-paralyzable due to the pulse shape, and the paralyzable due to the applied discrimination level). Nevertheless, corrections have not been applied, since we were interested in the limitations of the uncorrected pulse mode.

### 3.3 Campbell mode

In the Campbell, or fluctuation mode, the quantity of interest is the variance of the signal. Eq. (2.16) becomes

$$D^2(\eta) = s_0 \langle x^2 \rangle \int_{-\infty}^{+\infty} f(t)^2 dt \quad (3.2)$$

for the second order moment. The variance of the signal is approximated with the variance of the signal sample:

$$D^2(\eta) = \frac{N \sum_{i=1}^N X_i^2 - (\sum_{i=1}^N X_i)^2}{N(N-1)} \quad (3.3)$$

The observed variance is a sum of the variance of the real fission chamber signal triggered by the incoming neutrons, of the noise, and of the gamma and alpha contribution. One may measure the variance directly based on the sample values, or determine the integrate of the power spectral density of the signal. The amplitude of the pulses triggered by gamma radiation is much lower than the pulses emerging from fission events. Therefore, the gamma contribution is largely suppressed, because the amplitude term is squared [34].

The fluctuation mode requires calibration, meaning that the pulse and amplitude terms have to be determined. In the following simulations these terms were considered as known.

Fig. 3.4 shows the probability density function of the amplitude of simulated signals with and without noise at different count rates. For this illustration, a rather high noise level (20 %) was set to highlight the general effects of noise on the probability density function. The probability density function was calculated by normalizing the histogram of the sampled current values of the simulated signals. One can see that at lower count rates the density function and the variance of the noisy signal is mostly dominated by the noise. Hence, when the count rate is estimated based on (3.2), the variance of the noise biases the estimated count rate. Conversely, at higher count rates the noise does not have a great effect on the probability density function.

### 3.4 Current mode

In the current mode the quantity of interest is the mean current. In fact, the current mode is based on the first order Campbell equation:

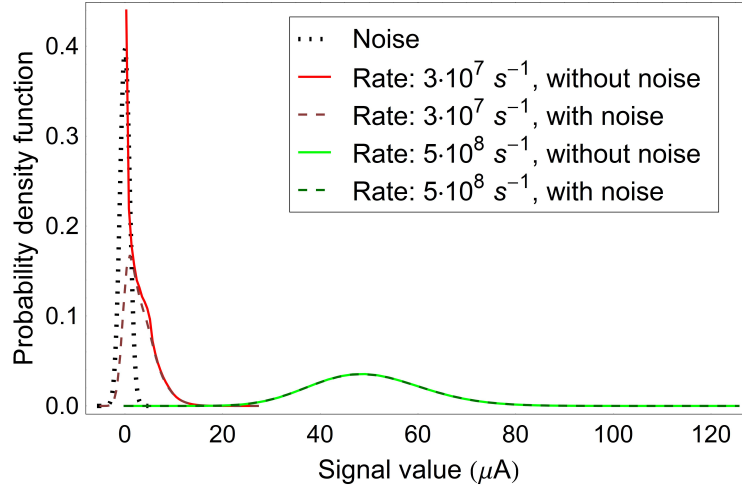


**Figure 3.4:** Probability density function of the signal.

$$\mathbf{E}(\eta) = s_0 \langle x \rangle \int_{-\infty}^{+\infty} f(t) dt \quad (3.4)$$

Since the pulse shape in (3.4) is normalized, the integral becomes unity, therefore the knowledge of the pulse shape is not necessary to calibrate a fission chamber in current mode, which makes the calibration relatively simple. Although, measuring the mean of the current is simple and robust, this mode is extremely sensitive to any unwanted signal contributions. In this work the current mode is not considered, since according to earlier studies the current mode does not provide a wider application range than the Campbell mode [6].

## 3.5 Linearity gap

An extensive numerical comparison between the pulse mode and the second order Campbell technique was performed. For the detailed results the reader is referred to Paper III.

In the simulations the pulses were considered as having an exponential decay shape with a width of around 90 ns. The performance studies were based on signal samples of 10 ms length with a sampling rate of 1 GHz. The signal was loaded with additional Gaussian white noise at various noise levels.

It was found that the pulse mode is nearly insensitive to the noise if the discrimination level is well set, whereas the Campbell is significantly biased by the noise at low count rates. Nevertheless, already a relatively narrow pulse amplitude distribution results in a count rate underestimation in the pulse mode, whereas the Campbell mode is not impacted by the stochastic amplitude if well

calibrated.

Fig. 3.5 shows the performance of the pulse and Campbelling modes for various pulse widths at a realistic noise level (the standard deviation of the noise is 5% of the pulse amplitude). The pulse width change was considered through changing the nitrogen content of the filling gas, which would have an impact only on the electron and ion velocity (see Fig. 2.3), but not significantly on the amount of induced electron-ion pairs by the fission fragment. Therefore, the delivered charge of the pulses (i.e. their integrals) was kept fix in the simulations, while changing the pulse width, which results in a change of the pulse amplitude.

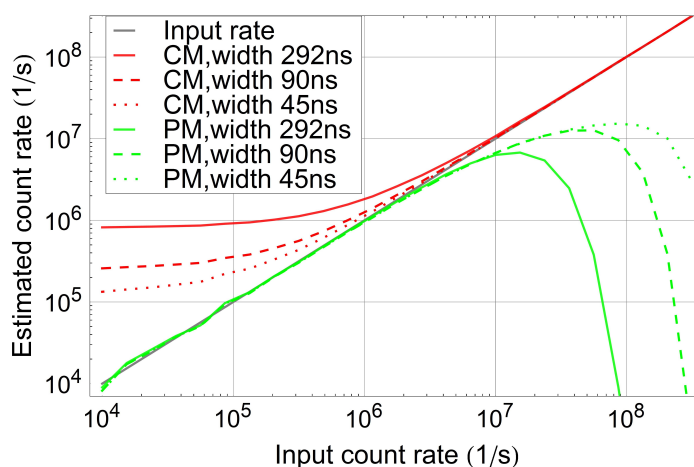


**Figure 3.5:** Impact of the pulse width on the pulse mode (PM) and the Campbelling (CM) (noise: 5%).

Fig. 3.5 shows that by increasing the count rate of the signal, the performance of the pulse mode gradually deteriorates, whereas the performance of the Campbelling improves (the reason for which is explained in Fig. 3.4). The pulse mode has a critical count rate, at which the dead-time saturates and the estimation breaks down. One can see that depending on the pulse width there will be a count rate region ( $10^6 - 10^7 \text{ s}^{-1}$ ), in which both methods fail to provide an accurate estimation. Although the literature of possible dead-time corrections is large and the research on correction methods is still active [35], most of the methods are cumbersome to be implemented in real-time systems and are limited to perform plausible corrections up to the breakdown point. Therefore, in order to guarantee the overlap of the applicability range of the pulse and the Campbell mode, the pulses have to be narrowed. As described in Chapter 2, this can be done by introducing nitrogen gas into the filling gas, but this solution would limit the lifetime of the chamber (due to the loss of nitrogen molecules under irradiation).

Thus there is a real need for unifying the two modes without altering the filling gas or the design of the chambers. A possible unifying solution is investigated in the following chapter.

## CHAPTER 4

# Performance of Higher order Campbelling

As the previous chapter highlighted, the traditional methods are vulnerable to the effect of various noises. The Campbell method is impacted by the parasitic noise of the electronic system. The gamma background and the ionic contribution results in a signal with rather high count rate, and low pulse amplitude, therefore it does not affect the pulse mode, but it has a moderate impact on the Campbell mode and a significant impact on the current mode. The alpha decay of the fissile layer induces relatively high pulses (the amplitude of pulses triggered by alpha particles is tenth of the amplitude of pulses triggered by the fission fragments) with a low count rate, therefore it impacts both the pulse, the Campbell and the current mode.

There are several solutions to reduce the impact of the various noises. The gamma and the alpha contributions can be compensated by introducing an additional ionization chamber in the measurement system with the same geometry, and containing an alpha decaying deposit instead of the fissile deposit (such as Ra-226), which emits an equivalent amount of alpha particles as the fissile deposit [36], and the measured mean and fluctuations of the compensating signal can be subtracted from the mean and variance of the fission chamber signal. On the other hand, the impact of the ionic contribution and the parasitic noise can be filtered by investigating the spectral properties of the signal [37]. Nevertheless these methods are not perfect, and introduce additional complexity to the measurement system, therefore reduce the robustness to interpret the signal and to detect sensor failures.

To remedy this problem, the application of the Higher Order Campbelling (HOC) methods was proposed [20, 38]. These use the higher order statistics (cumulants) of the detector current to estimate the detection rate. Although the theoretical relationship between the higher order cumulants and the mean detection rate has long been known, the applicability and performance of these methods in practical applications and in transient scenarios has not been extensively tested, and the uncertainty related to applying high order methods has not been addressed. The available experimental results have large uncertainties, and the measurements need relatively long (a few s) signal samples [39], which is unfavorable for real-time applications. The rapid development of digital measurement devices (such as FPGAs) brings recent attention to these methods, since the reliable estimation of the higher order moments of the signal became achievable.

This chapter provides an introduction to and summary of the numerical and experimental performance studies of the HOC method detailed in Paper IV and Paper V.

## 4.1 Higher order Campbelling

Let us rewrite (2.16) in a general form:

$$\kappa_n^{(st)} = s_0 \langle x^n \rangle = s_0 \int_{-\infty}^{+\infty} f(t)^n dt = s_0 \cdot C_n \quad (4.1)$$

where commonly, the methods in which  $n \geq 3$  are called higher order methods. Eq. (4.1) shows that if the pulse shape  $f(t)$  and the amplitude distribution  $w(x)$  are known (therefore the calibration coefficient  $C_n$  is determined), and the cumulant  $\kappa_n$  (of any order) of the signal is determined from measurement, then the count rate  $s_0$  of the signal can be estimated.

### 4.1.1 Cumulant estimation

In practice, the empirical distribution of the signal is estimated from a finite, discrete sample, with an uncertainty depending on the length of the signal sample, as illustrated in Fig. 4.1. As a consequence, the cumulants of the signal have to be also estimated, and the estimations have uncertainties as well.

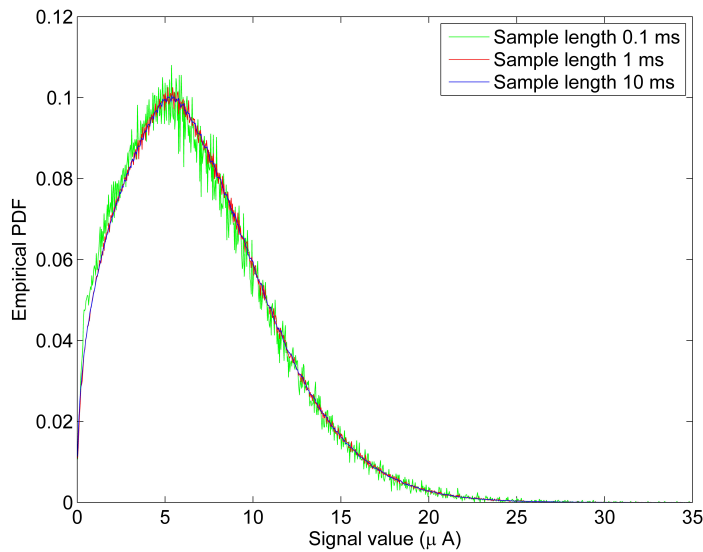


**Figure 4.1:** Empirical probability density function depending on the signal length (with identical sampling rate).

For the current work the k-statistics were applied to estimate the cumulants [40]. The  $n$ th k-statistic  $k_n$  is a unique symmetric unbiased estimator of the cumulant  $\kappa_n$ , defined such that

$$\langle k_n \rangle = \kappa_n \quad (4.2)$$

If the sum of the  $n$ th powers of the data points  $S_n$  is defined as

$$S_n = \sum_{i=1}^N X_i^n \quad (4.3)$$

where  $N$  stands for the size of the sample as in the previous chapter, then the first two higher order k-statistics can be given in terms of these sums as

$$k_3 = \frac{2S_1^3 - 3S_1S_2 + N^2S_3}{N(N-1)(N-2)} \quad (4.4)$$

and

$$k_4 = \frac{12NS_1^2S_2 - 3N(N-1)S_2^2 - 4N(N+1)S_1S_3 + N^2(N+1)S_4 - 6S_1^4}{N(N-1)(N-2)(N-3)} \quad (4.5)$$

The convergence of the cumulant estimation to the real value of the cumulant is the subject of Sec. 4.2.1.

## 4.2 Numerical studies

First, the performance of the higher order methods was investigated through numerical simulations. In this regard the convergence of the cumulant estimations was studied and the optimal measurement time was defined. Then, the impact of the ionic pulses, the parasitic noise of the electronics and the competitive shot noises were determined for the traditional and higher order Campbell methods, in order to decide how large gain can be achieved by applying very high orders.

In the numerical study a normalized damped exponential pulse shape was considered for describing the electronic and ionic pulses:

$$f(t) \propto e^{-t/p_1} - e^{-t/p_2} \quad (4.6)$$

For the quantitative work, reference pulse parameters were chosen to describe both the electronic and the ionic pulses. The characteristics of the pulses are summarized in Table 4.1. The pulses were chosen to have deterministic length and shape: although, for a given pressure, there is some variation in the pulse shape (depending on the angles of the ionization tracks, and the kinetic energy of the

**Table 4.1:** The reference pulse characteristics

type	e <sup>-</sup>	ion
time parameter $p_1$	20 ns	2 $\mu$ s
time parameter $p_2$	4 ns	0.4 $\mu$ s
mean charge $\langle q \rangle$	0.1 pC	0.1 pC
amplitude $a$	3.34 $\mu$ A	34 nA
pulse width	100 ns	10 $\mu$ s
resolution	1 ns	1 ns

fission fragment), for simplicity, here only a mean shape is considered, since the reference fission chamber (CFUL01) is relatively small (the gas gap is only 2 mm), therefore, the pulse width is roughly independent of the track of heavy ions for this fission chamber.

For each investigation, 1000 signals with the same measurement time were generated in order to assess the random error of the estimated count rate. The expected value, or mean, of these estimations reflects the systematic error caused by the noise.

### 4.2.1 Convergence

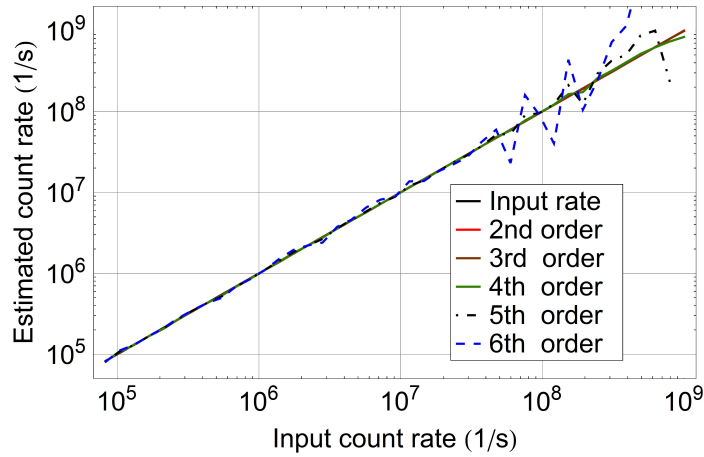
Fig. 4.2a illustrates the count rate estimation of several order Campbell methods based on 10 ms long signal samples without noise (the second, third and fourth order estimations overlap each other). One can immediately see that at higher count rates the higher the order of the method is, the higher the uncertainty of the estimation is. The reason is the increase of the associated variance of the estimators

$$var(k_n) = \langle (k_n - \kappa_n)^2 \rangle \quad (4.7)$$

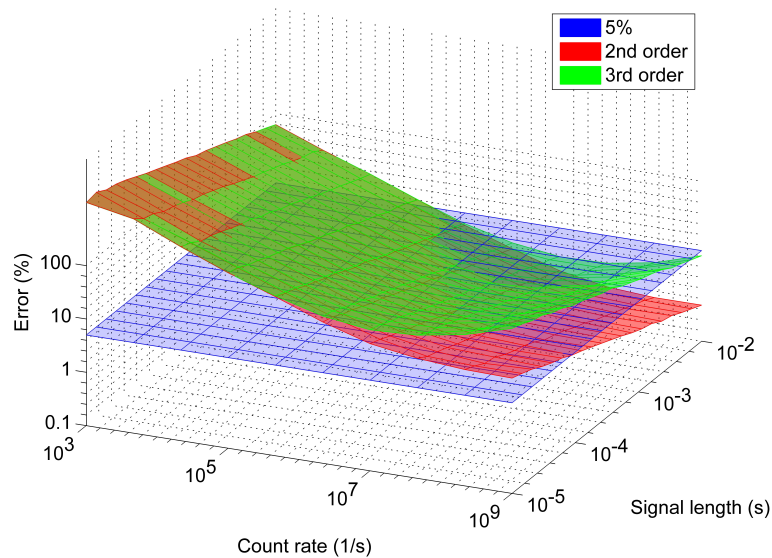
The analytic form of this variance and the unbiased estimators of the variance can be found in the literature [40]. Here only a illustrative term is highlighted.

$$var(k_n) \propto \frac{\kappa_2^n}{N} \quad (4.8)$$

Eq. (4.8) means that the variance of the estimator is proportional to the  $n$ th power of the variance of the signal. Since the variance of the signal increases with the count rate (which is expressed by the traditional Campbell equation introduced in Eq. (3.2) and illustrated in Fig. 3.4), the variance of the estimation increases exponentially with the count rate. This means that for accurate measurements with higher orders, one needs longer measurement times. Since for real-time monitoring one attempts to have as short measurement times as possible, this criterion limits the application of the very high order methods.



(a) Illustration of the estimation uncertainty.



(b) Random error of the count rate estimation.

**Figure 4.2:** Error of the Campbell estimations.

Instead of evaluating the formulae of the variance of the estimators, a rather pragmatic approach was applied, which inherently includes the uncertainties due to the randomness of the process. Many signals were created at several count rates with several measurement lengths, and the relative difference of the estimated and the real count rate was determined. The random error of the estimation was defined as the standard deviation of this set of differences. The results are summarized in Fig. 4.2b for the second and the third order. One can see that at high count rates the random error indeed exponentially increases; and further, that at lower count rates, the error also increases, due to the randomness of the process. The plane related to 5% error is also shown in the figure as a reference.

Based on these results it was concluded that for the third order methods a measurement time around 1 – 10 ms provides reliable count rate estimation over a wide count rate range (above  $10^4 - 10^5 \text{ s}^{-1}$ ). Therefore, in the continuation, the computations were done for 10 ms.

Although, in the figure the fourth order estimate is not included, the calculations showed that the fourth order encounters more serious convergence problems. Nevertheless, in some of the following results the fourth order estimations are also included, to point out whether the application of higher than third order estimations has any practical advantage.

### 4.2.2 Noise suppression

This section investigates the impact of the ionic pulses, the parasitic noise of the electronics and the competitive shot noises (i.e. the gamma and the alpha contribution). These noises cause systematic measurement errors since the calibration coefficient in Eq. (4.1) takes into account only the most dominant part of the signal, the electronic pulses, because in an experimental calibration one determines the electronic pulse shape (as shown in Sec. 4.3). On the other hand, the measured cumulant is related to the compound signal (i.e. the fission chamber signal and the various noises). Hence, the systematic error may be estimated analytically (an example is given in Paper IV for the ionic contribution). Nevertheless, in the numerical simulations, the random errors due to the fluctuation of the number of pulses  $N(t)$  arriving during the measurement time and the variance of the cumulant estimations are inherently included. Therefore, with simulations one gains more understanding about the significance of the impacts of the noise.

As was seen in Table 4.1, the ionic pulses carry the same amount of charge as their electronic counterparts, but their width is around two orders of magnitude longer, therefore the amplitude is two orders of magnitude lower. Figs. 2.4 and 2.5 have illustrated that such ionic contribution will introduce a low frequency noise.

Both analytic and numerical results (as presented in Paper IV) show that the traditional Campbell mode overestimates the count rate with about 1.2 % due to the ionic contribution, whereas the third order Campbell mode can reduce this bias to 0.2 %. Nevertheless, due to the larger random errors of the third order method, at count rates higher than  $10^8 \text{ s}^{-1}$  this reduction benefit vanishes.

The components of the electronics (such as the pre-amplifier, the cables and the connections) introduce a parasitic noise to the signal. Several simulations were carried out assuming different frequency dependence of this noise, since the experimental work shows that the noise is not white. From measurements, it was also verified that the noise distribution is close to Gaussian and its standard deviation is around 6-7 % of the mean pulse amplitude. It was shown that both the third and fourth order methods sufficiently suppress the impact of the noise, as the higher order cumulants of the Gaussian distribution are zero. The application

of the fourth order does not bring any advantage over the third order method. In contrast, the higher order methods are not entirely insensitive to the noise of the electronics: as shown in Eq. (4.8), a signal distribution with larger variance increases the variance of the estimator, therefore higher noise levels increase the random error of the higher order methods. For realistic noise levels this effect does not play a significant role, but it can be concluded that to suppress parasitic noise, it is favorable to limit the order of the method to avoid increasing the random error.

In the fission chamber other, not neutron-triggered ionizing radiations also induce pulses. These pulses also create a shot noise in the chamber, referred in this thesis as competitive shot noise. The main undesirable contribution originates from gamma radiation [41] and the alpha decay of the deposit. The assessment of the gamma contribution to the signal of a fission chamber, located in the reflector region of a sodium cooled reactor, lies beyond this work, nevertheless, the gamma triggered pulses are assumed to have at least 2 orders of magnitude lower pulse amplitude than the pulses of the fission fragments [41]. On the other hand, the alpha contribution of the reference fission chamber CFUL01 can be easily evaluated, hence the impact of the alpha background can be estimated. Since the deposit contains around 1 g of uranium (with a U-235 enrichment of 90 %), the alpha count rate is around  $10^5 - 10^6 \text{ s}^{-1}$ . The mean pulse amplitude of the pulses triggered by the alpha particles was studied with the pyFC tool, and is around 10 % of the mean pulse amplitude of the pulses triggered by the fission products. Since both the gamma and the alpha pulses are mostly covered by the noise of the electronics, it is not possible to consider them in the calibration procedure.

With numerical simulations it was shown that, regarding the competitive noise, by increasing the order of the method, a significant suppression gain can be achieved (see Paper IV for further details). However, the random error of the fourth order exceeds its systematic error reduction compared to the third order. With the third order mode the competitive shot noise can be successfully suppressed even if the parasitic pulse amplitudes are 25 % of the neutron triggered pulse amplitudes and the intensity of the competitive process is comparable with the intensity of the neutron signal.

As a summary, Fig. 4.3 presents the results of the systematic and random errors for signals where all the above-mentioned noises appear simultaneously: Gaussian noise (with a standard deviation of 6 % of the mean pulse amplitude), ionic signal and competitive shot noise (with the same count rate as the fission rate - which is an underestimation for the alpha count rate at higher than  $10^6 \text{ s}^{-1}$  fission rates -, and the competitive pulse amplitudes are 1 % or 10 % of the mean pulse amplitude triggered by neutrons).

In case the count rate of the non-neutron triggered pulses is comparable with the count rate of the neutron-triggered pulses for the HTFCs applied in Astrid, and further if the data acquisition system can filter out low frequency noises (such as the ionic contribution), then at high count rates (above  $10^8 \text{ s}^{-1}$ ) still the application

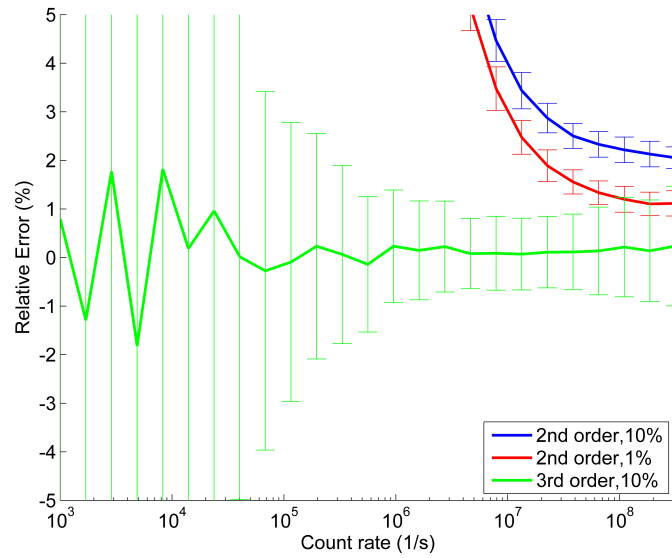


**Figure 4.3:** Cumulative impact of noise.

of the second order method may be advisable, considering the larger random error of the third order estimation.

### 4.2.3 Transient

As detailed in Chapter 2, reactor transients result in an inhomogeneous signal, in which the count rate of the signal can be described as a time dependent function  $s(t)$ . The developed simulation toolbox has included the capability of describing such continuously changing count rates.

In order to assess the dynamic response of the higher order Campbelling, a test scenario was considered, which describes a heuristic, fast change in the count rate. The count rate was increased from  $10^5 \text{ s}^{-1}$  to  $10^8 \text{ s}^{-1}$  in 50 ms, and after reaching the maximum, it decreased to  $10^5 \text{ s}^{-1}$  in 50 ms (illustrated by the solid line in Fig. 4.4; note the logarithmic scale on the y-axis).

The simulation was performed as taking consecutive finite samples of the signal, and estimating the count rate of them with the Campbell equations for homogeneous processes (Eq. (4.1)). This implies that the inhomogeneous signal was approximated as a sequence of quasi-homogeneous signals. The length of the consecutive samples (the estimation window) was set to 1 ms or 10 ms.

Fig. 4.4 presents the count rate estimation over the transient event for the different estimation windows. The results show that there is a delay of the estimation due to the length of the sample size. If the window size is set too short then the accuracy of the measurement is going to be worse (due to the random error related to the stochastic characteristic of the signal and to the inaccuracy of the third order

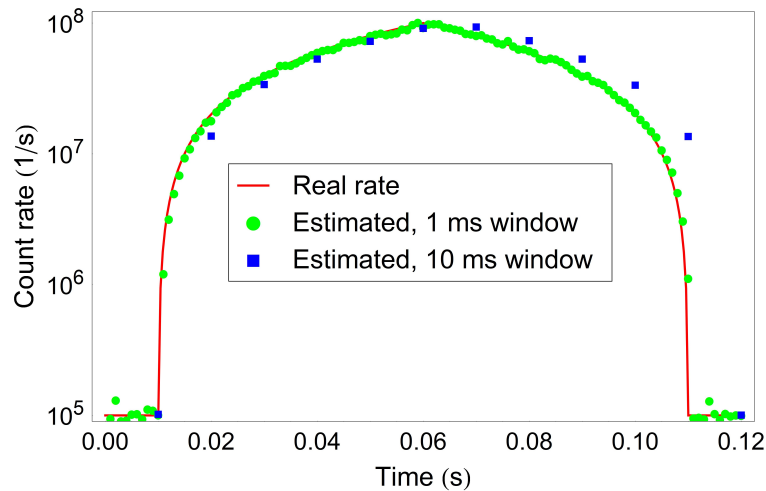


**Figure 4.4:** Transient simulation: count rate estimation with window sizes 1 ms and 10 ms.

estimation), whereas with longer measurement times the exact shape of the transient may be lost, as in the example with longer measurement window, the peak is missed. This means that if the sample window is well optimized (meaning that it is sufficiently long to guarantee an accurate cumulant estimation, but sufficiently short to monitor the change in the count rate), then the inhomogeneous signal can be approximated as a sequence of homogeneous signals, and the homogeneous Campbell equations can be applied.

It can be concluded that the monitoring of transients is limited by the shortest reliable measurement time (in which the estimation is converged). As illustrated, with rather short, 1 ms long windows it is possible to reach a fair estimation even at high count rates, which means that one can be confident that transients slower than the ms scale can be followed with third order Campbell methods.

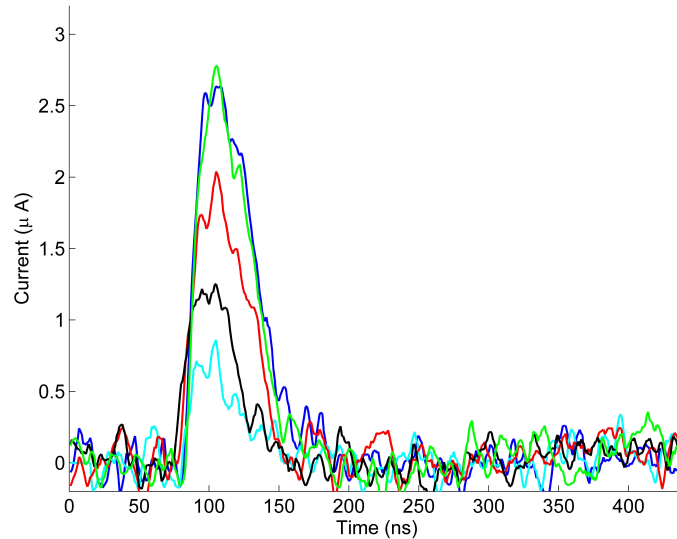
### 4.3 Experimental studies

In order to verify experimentally the wide range linearity of the third order Campbell method, the possibility of calibration and the possibility to monitor transient events, a measurement campaign was carried out (the details of the experimental setup are described in Sec. 2.3.3).

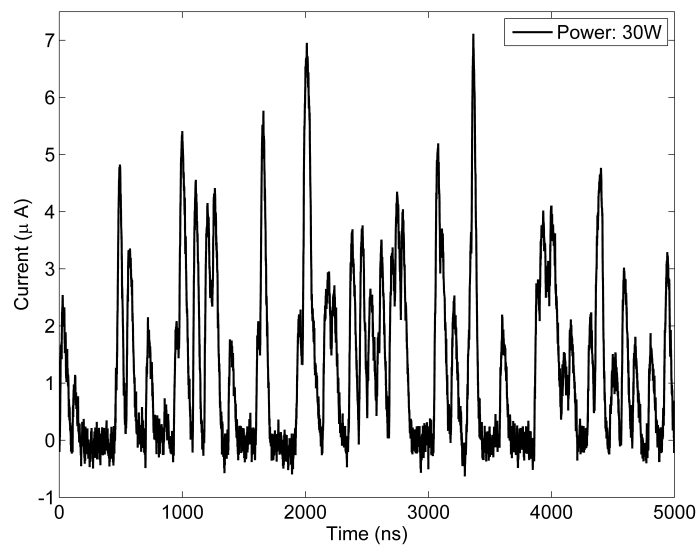
At low reactor power levels when the pile-up of pulses is unlikely, pulses were collected separately (a sample of the recorded pulses are available in Fig. 4.5a). Although, at such low power levels the pile-up events are rare, during the post-processing the incidental pile-up events were eliminated from the data set.

At medium and high power levels, 10 ms long signal samples were collected (such a measurement at 30 W power level is illustrated in Fig. 4.5b). At medium levels the pulses overlap moderately. This provides an opportunity to estimate

the count rate accurately with pulse counting techniques and to compare it with the estimation obtained from the calibrated HOC mode.



(a) Sample of recorded pulses.



(b) Sample of recorded signal at 30 W.

**Figure 4.5:** Illustration of recorded data.

### 4.3.1 Calibration and linearity

The separated pulses recorded at low power were studied in order to determine the calibration coefficient  $C_n$  (introduced in Eq. (4.1) as the product of the integral

of the  $n$ th power of the mean pulse shape and the  $n$ th order raw moment of the pulse amplitude distribution) for the second and the third order. The measured mean pulse shape and its standard deviation are shown in Fig. 4.6. A slight bump follows the main pulse, which is an artifact due to the current bouncing back on the cable.

The measured calibration coefficients of the second and third order Campbelling mode are summarized in Table 4.2. It has to be highlighted that these coefficients belong to the whole experimental setup (but are independent from the neutron spectra) and not only to the fission chamber. The random error of the coefficients was determined empirically (i.e. the coefficient was calculated for 10 set of 10000 pulses). The systematic error of the coefficient was estimated from the error of the amplitude measurement, since during the measurement, a discrimination level has to be introduced to separate the pulses from the noise. Therefore pulses lower than the discrimination level are not accounted for in the calibration procedure. Table. 4.2 also contains the empirical third order calibration coefficient  $C_{3,empir}$ , introduced later.

Since, as previously described in Chapter 2, the CFUL01 fission chamber is a multi-coated fission chamber, the impact of the variation in pulse shapes coming from the different coatings was addressed in Paper V. The overall error of the calibration coefficient due to assuming that all pulses have the same shape was estimated to be around 3 %.

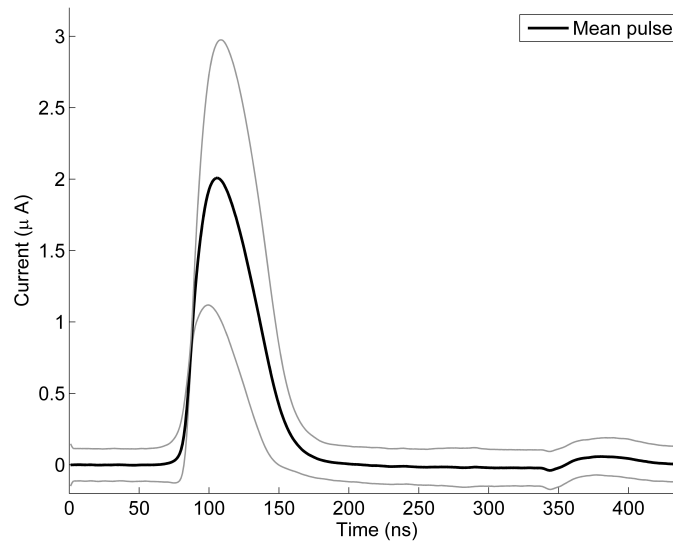


**Figure 4.6:** The recorded mean pulse shape and its standard deviation.

To assess the linearity of the third order Campbelling, several signal samples were recorded at 28 different power levels between 0.2 W and 80 W. This allowed to estimate the deviation of the cumulant estimation as well.

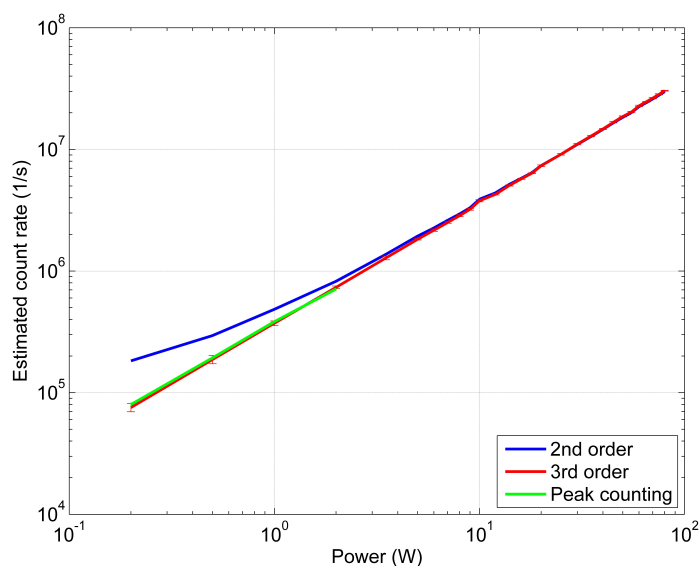
The count rates of the signals taken below 2 W were estimated with pulse count

**Table 4.2:** Calibration coefficients

	mean
$C_2 (A^2 Hz^{-1})$	$(2.00 \pm 0.04) \cdot 10^{-19}$
$C_3 (A^3 Hz^{-1})$	$(5.32 \pm 0.3) \cdot 10^{-25}$
$C_{3,empir} (A^3 Hz^{-1})$	$(5.19 \pm 0.2) \cdot 10^{-25}$

algorithms as well. These made it possible to compare the count rate estimations of the calibrated third order method to the estimations of the pulse counting (which can be considered as a reference at low count rates) and to determine an empirical calibration coefficient  $C_{3,empir}$  by fitting a linear model between the empirical pulse count and the third order cumulant estimations. The empirical calibration coefficient is included in Table 4.2.

The count rate estimation results are summarized in Fig. 4.7. One immediately notices the failure of linearity for the traditional Campbelling at low count rates. However, the count rate estimated by the third order cumulant shows good agreement with the results of the pulse counting, and the third order Campbelling provides a linear estimation over the whole power range.

**Figure 4.7:** Count rate estimation with different methods.

The good agreement between the empirical and HOC calibration verifies the possibility to calibrate the fission chambers in HOC mode empirically. Thus, if one can perform a reliable pulse count estimation at low count rates, then the empirical calibration provides the simplest and most robust calibration methodology (i.e. the difference in pulse shape will not have any significance and the cumulant measuring system can be cross calibrated with a reliable pulse counting system, thus the system does not need to be capable of recording the signal). Such a calibration is not plausible for the traditional Campbelling method, due to the linearity gap

between the pulse counting method and the second order Campbelling.

### 4.3.2 Transient

The numerical studies showed that higher order Campbelling methods are limited only by the smallest reliable measurement time to monitor fast transients. In the frame of the measurement campaign, an experimental demonstration of the transient monitoring was performed.

The MINERVE reactor is not designed to induce transients, therefore the fastest transient which can be authorized by the operators is the control rod drop transient. For the current measurement, the reactor power was kept at a stationary 60 W power level, when the control rods were dropped. The fall of the control rods takes around 0.4-0.5 s.

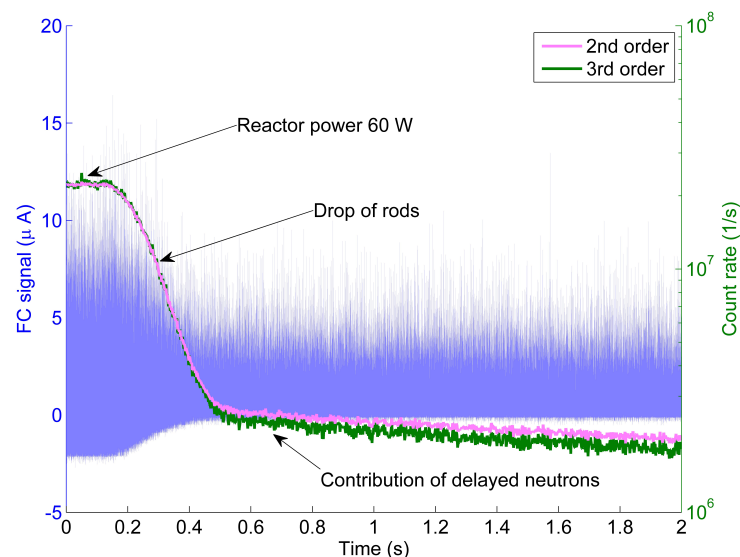


**Figure 4.8:** Transient measurement.

Fig. 4.8 shows the time evolution of the Campbell count rate estimations based on consecutive, 2 ms long signals (right axis, pink and green curves in the foreground) and the fission chamber signal (left axis, light blue curve in the background). Since the applied pre-amplifier removes the mean of the signal, one can observe the change of the offset during the measurement. At the beginning of the measurement the reactor was in stationary state, hence the estimated count rate is constant in time. The control rod was dropped 0.1 s after the recording started, which results a rapid, exponential decrease of the count rate. The control rod was fully inserted after a fall of 0.4 s, when the decrease of the count rate is turning slower, and the pulses in the signal are mostly triggered by the delayed neutrons. Both the traditional and the third order Campbell methods show a

sufficiently dynamic response during the fall of the control rod. However, at the end of the transient the count rate is overestimated by the traditional Campbelling.

## 4.4 Concluding remarks on the higher order Campbelling

It was shown through numerical studies that the uncertainty of the higher order cumulant estimations limits the applicable order.

Nevertheless, it was seen that already the third order method achieves significant noise suppression capabilities: it sufficiently eliminates the impact of the ionic signal contribution, the parasitic noises of the measurement system and possible competitive shot noises (such as the gamma background, and the alpha radiation of the fissile coating). Nevertheless, due to the large random error of the third order estimation at high count rates, it is advisable to apply a system, which makes use of the second order estimation at count rates above  $10^9 \text{ s}^{-1}$ .

It was shown that with the currently available digital sampling rates it is possible to achieve accurate measurements above  $10^4 \text{ s}^{-1}$  based on signal samples of a few ms. Monitoring lower count rates is still possible, but the measurement time needs to be longer (nevertheless, the pulse mode has the same drawback).

The wide range linearity and the transient following capability of the third order Campbell mode was verified through an experimental campaign.

Determining the theoretical calibration coefficient in high order mode may be problematic with cumulant measuring systems, which are not capable of recording the signal. For such systems, the pulse recording has to be done with a separate apparatus, which may have a different transfer function. In order to overcome this issue, it was verified that the calibration is possible empirically, based on pulse counting techniques.

## CHAPTER 5

### Self-monitoring

Eq. (4.1) shows that the cumulants of the signal may change not only due to the change in the count rate, but also due to the change in the mean pulse shape or the pulse amplitude distribution. The higher order methods are particularly sensitive to such changes due to the higher exponents in Eq. (4.1). These changes may occur due to the reduction of detector filling gas pressure or voltage. During measurements, only the change of the cumulant (therefore the change of the estimated count rate) will be detected, thus we have to be able to decide whether this change occurred due to the change of the neutron flux around the detector or due to the malfunction of the detector.

The current chapter explores the possibility of detecting the detector failure from the change of the shape  $f(t)$  of the detector pulse. Namely, earlier work showed how the temporal auto-correlation of the detector signal depends on the detector pulse shape [42]. Hence, if the detector malfunction results in a change of the detector pulse shape, this latter can be discovered from the detector signal auto-correlation function, or from its power spectral density. Thus, this chapter investigates the alteration in the mean pulse shape due to failure of the detector and investigates the possibility to identify the malfunction from the changed characteristics of the detector signal PSD. In this thesis the capability of identifying such failures is called self-monitoring or smart detector capability.

Previously there have been attempts to perform regular tests to identify malfunctions of fission chambers. Ref. [43] proposed periodic testing (at least annual) of fission chambers installed in a reactor, and tests of newly-manufactured chambers and stored spare chambers. This pioneering technique was based on analog measurements of the power spectral density, and identifying changes in the amplitude of the spectra (therefore, the measurements had to be taken at steady flux level). An other proposition was to measure the transition frequency between the ion and electron plateau (i.e. the inflexion point in Fig. 2.5), which is not straightforward in case one wants to perform real time measurements (the change which has to be detected is a few kHz), and may be problematic if the instrumentation filters the frequencies lower than a few kHz, and if the measurements are not sufficiently long. To investigate these properties one needs dedicated offline measurements.

In contrast, Paper VI quantifies how the width of the spectra (i.e. the length of

the electron plateau) changes during a malfunction, and focuses on the possibility of real-time application, i.e. the possibility of performing spectral analysis during the operation. For this purpose the investigation of the amplitude of the spectrum is not adequate, since that may change due to the change in the reactor power as well.

## 5.1 Hypothetical malfunction

As mentioned before, the change of the fission chamber characteristics may have several causes. An illustration is given in Paper VI, where the chosen scenario was a pressure drop of the filling gas due to a crack on the wall of the fission chamber. Such a crack would not appear instantaneously, rather would develop during a longer period of time. Modeling the temporal development of such ruptures is beyond the scope of this thesis.

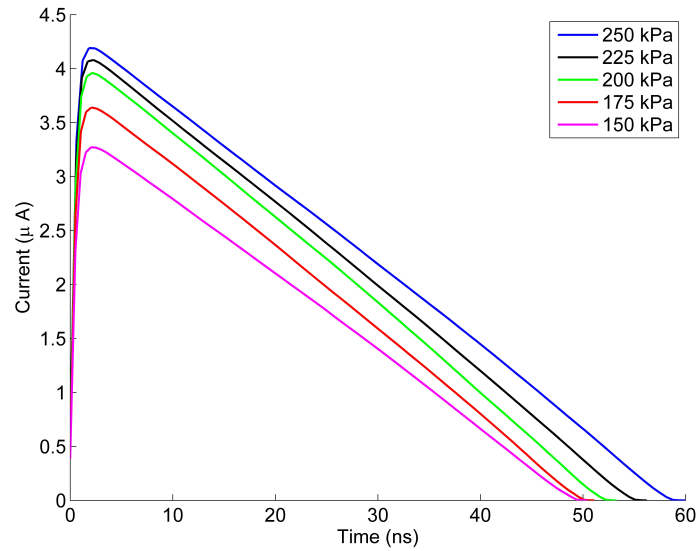
The sodium pressure in an Astrid-like core at the fission chamber location was calculated with Bernoulli's theorem and was found to be 72 kPa. This implies that the filling gas would leak from the chamber in case of a rupture. The characteristic time of this leakage strongly depends on the size of the crack, but for microscopic ruptures (a few tens of  $\mu\text{m}$ ) the leakage progresses for a few hours. The goal of the present work was to quantify the minimum pressure drop which can be detected, in order to assess whether early fault detection is possible.

For this work the CFUL01 fission chamber was the reference fission chamber.

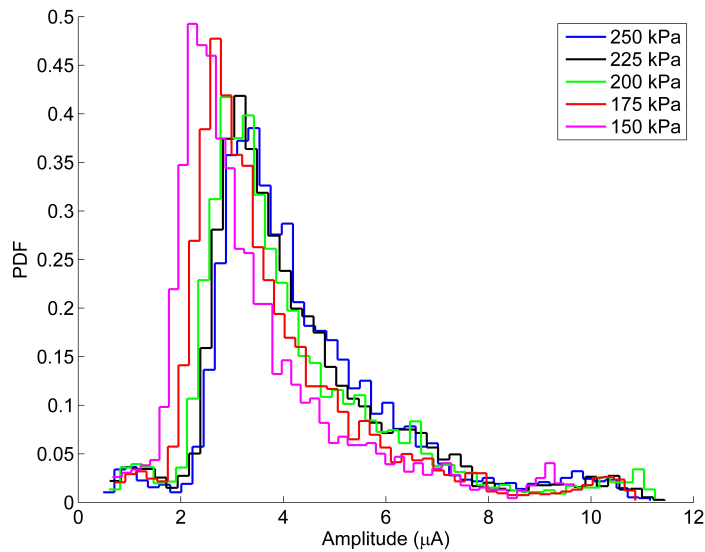
## 5.2 Impacts of pressure drop

First the pyFC suite was applied to simulate the change of the pulse shape during the pressure drop. The computation of the mean pulse shape and that of the pulse amplitude distribution was performed for several pressure values between 150 kPa and 250 kPa. As described before, although, for a given pressure, there is some variation in the pulse shape (depending on the angles of the ionization tracks), for simplicity, in the following only the mean shape is considered, because the most important characteristics of the pulse, its width, is roughly independent of the track (since the CFUL01 chamber is only few mm in diameter).

The results are summarized in Fig. 5.1. By decreasing the filling gas pressure (and therefore the number of gas atoms in the chamber) the pulse width and the carried charge (the integral of the current pulse) is decreasing as well. At lower pressure the heavy ion creates less electron-ion pairs and the mobility of the electrons becomes higher. The change in the mean pulse shape can be observed in Fig. 5.1a. The pulse width shows a saturation which is a consequence of the saturation in the drift velocity at low pressures (as shown in Fig. 2.3).



(a) Mean pulse shape.



(b) Amplitude distribution.

**Figure 5.1:** Fission chamber pulse characteristics due to pressure drop.

Fig. 5.1b shows that the amplitude distribution of the created pulses is also affected by the pressure drop. The median of the distribution becomes lower and the raw moments of the distribution are decreasing during the pressure drop, since there is less gas to be ionized.

As a consequence, both terms of the calibration coefficient, introduced in Eq. (4.1), are decreasing during the pressure drop. The alteration in the second and third order coefficient is -15 % and -21 %, respectively, due to 25 kPa pressure change. Therefore the cumulants of the signal decrease significantly, even if the

real count rate is unchanged. This results in an underestimation of the count rate with the original calibration coefficient. As shown in Fig. 5.2, the count rate estimation drops during the pressure loss, even though the reactor is in a steady state.

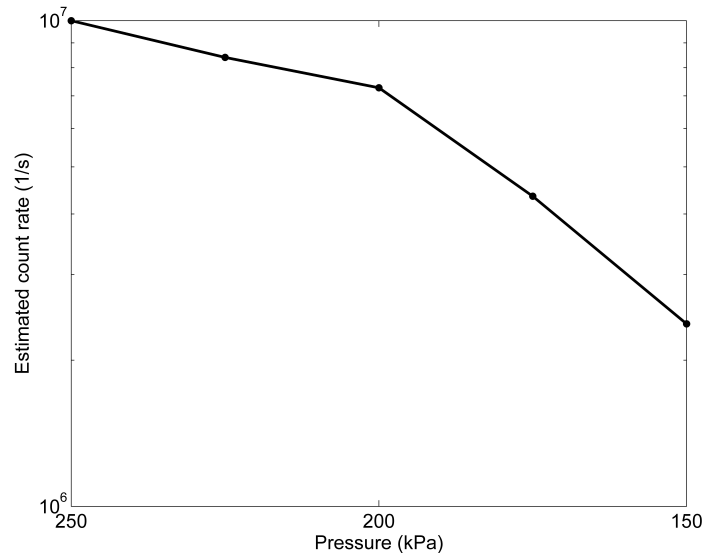


Figure 5.2: Estimated count rate at  $s_0 = 10^7 \text{ s}^{-1}$ .

### 5.3 Fault indicator

The task of a self-diagnosing detector is to identify whether the estimated count rate changed due to the change of the count rate or due to other reasons.

Therefore we have to define a measurable quantity of the fission chamber signal which is sensitive to the pulse shape change but not to the count rate change. The power spectral density of the detector signal satisfies this requirement. For a filtered Poisson process, it can be shown that the power spectral density has a breakdown at high frequencies which depends on the pulse shape [42].

To study the PSD of fission chamber signals, the same fission chamber signal simulator was used as in the previous chapters. With the software, various pulse trains, related to different filling gas pressures, were simulated.

First, it was verified that changing the count rate of the signal does not effect the shape and the breakdown frequency of the PSD, just the amplitude. Also the impact of the pulse amplitude distribution was studied separately. In accordance with our expectations, the pulse amplitude distribution has only an effect on the amplitude of the PSD.

Finally, the impact of the pulse shape was investigated. The results are shown in Fig. 5.3. Due to the alteration of the pulse shape, primarily of its width, the PSD

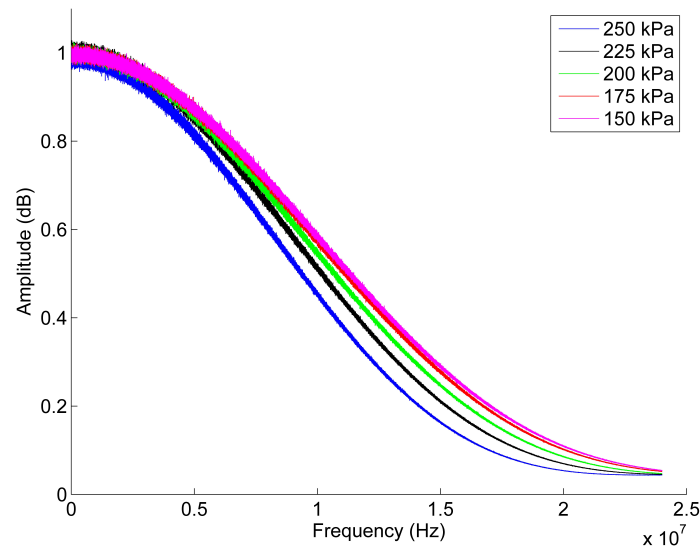


**Figure 5.3:** PSD of the signal at different filling gas pressures.

will extend to higher frequencies at lower filling gas pressures. This change was quantified by defining the PSD width as its full width at half maximum (FWHM) to provide a simple and measurable quantity to indicate gas leakage. The PSD width is contained in the 5-15 MHz band, which is an easily accessible frequency band with modern instrumentation.

One can notice that the spectral densities in Fig. 5.3 have some variance, therefore the estimation of the FWHM is not trivial. To guarantee reliable FWHM estimation and therefore reliable fault detection, the accuracy of the method had to be assessed. It was found that in case the FWHM estimation is based on 10 s long measurements, the error of the estimation is less than 1 %, which corresponds to a minimum detectable pressure drop of 5 kPa.



## CHAPTER 6

# Implementation of the measurement techniques

In the previous chapters the signal processing was performed offline: after recording the signal, it was post-processed with a PC. Nevertheless, the ultimate goal of neutron monitoring is to realize a system, which is capable to work online.

Recently, neutron flux monitoring systems based on the traditional Campbell technique make use of digital components, and FPGAs [31, 44]. Also the HOC methods were implemented on digital measurement devices with low sampling rate [39]. Nevertheless, there is still need to develop a neutron flux monitoring system, which is capable to work in real-time, and to provide count rate estimation based on ms long signals.

In case of higher order Campbell, the online capability would mean that the higher order sums (introduced in Eq. (4.3)) are computed and the cumulants are estimated in real-time, while recording the signal. Therefore, the development of a prototype board, which implements the higher order Campbell technique and the self-monitoring capability in real-time was started.

This chapter summarizes Paper VII, which covers the implementation of the real-time higher order Campbell method on a the prototype measurement board. The requirements of an online neutron monitoring system, and the challenges of the implementation are summarized, and finally some of the experimental results are highlighted.

### 6.1 Requirements of real-time measurements and hardware selection

A recent trend to combine field-programmable gate arrays (FPGA) with embedded microprocessors and related peripherals in order to create a system on a programmable chip (SoC), made the development of digital measurement systems simpler and affordable. Currently several such systems are available on the market with varying complexity.

For the work the Red-Pitaya board [45] was chosen. The Red-Pitaya board was created in order to provide a customizable measurement system. The board comes

with a large amount of open source examples and tutorials, in order to facilitate implementing new modules. Its low price and a relatively large user community makes it an adequate tool to build a prototype system.

The requirements to build a real-time fission chamber signal processing system (and the characteristics of the board in relation to the requirements) are the following:

Requirement	Red-Pitaya
Capability to convert and process the signal at the output of the available pre-amplifier which is typically a voltage between -10 V and 10 V.	Board provides two measurement ranges through jumper positions: $\pm 0.6$ V and $\pm 16$ V.
High sampling frequency in order to resolve the signal consisting of pulses with a width of a few tens of nanoseconds.	Board hosts ADC with 125 MHz sampling
Real-time computation of the first, second and third order sums of the signal.	FPGA on board
Ability to process a large amount of data in real-time (given that a time window of a few ms has to be applied for accurate estimations).	FPGA on board

The Red-Pitaya board is built around a Xilinx Zync 7010 SoC which embeds an FPGA and a dual core Arm CPU. It hosts two Analog-to-Digital Converters (ADC) and two Digital-to-Analog Converters (DAC) which are directly connected to the FPGA. The ADCs have a sampling frequency of 125 MHz and a resolution of 14 bits. The board provides two measurement ranges through jumper positions:  $\pm 0.6$  V and  $\pm 16$  V. The great advantage of the FPGA is the possibility to design a circuit, which allows to process the data on-line, therefore reducing the time, and the memory storage needs for heavy computations. This makes FPGAs ideal to perform simple computing patterns on a vast amount of data in real-time. These characteristics of the Red-Pitaya fulfill all the above stated requirements to develop an online neutron monitoring system: the board is able to process the signal at the pre-amplifier output (which is  $\pm 10$  V for the pre-amplifier applied in this work), to resolve the fission chamber pulses (with a length of few tens of ns), and to perform the real-time processing of a large amount of data.

## 6.2 Implementation of HOC

The main task of the system is to evaluate the third order cumulant estimator  $k_3$  (Eq. (4.4)), which involves the computations of the sums  $S_1$ ,  $S_2$  and  $S_3$  (Eq. (4.3)).

Stages \ Clock	$i - 1$	$i$	$i + 1$	$i + 2$	$\dots$	$N + 2$
ADC in	$X_{i-1}$	$X_i$	$X_{i+1}$	$X_{i+2}$	$\cdot$	$\cdot$
$X$	$\cdot$	$X_{i-1}$	$X_i$	$X_{i+1}$	$\cdot$	$\cdot$
$X^2$	$\cdot$	$X_{i-1} \cdot X_{i-1}$	$X_i \cdot X_i$	$X_{i+1} \cdot X_{i+1}$	$\cdot$	$\cdot$
$S_1$	$\cdot$	$S_1 + X_{i-1}$	$S_1 + X_i$	$S_1 + X_{i+1}$	$\cdot$	$\cdot$
$X^3$	$\cdot$	$\cdot$	$X_{i-1}^2 \cdot X_{i-1}$	$X_i^2 \cdot X_i$	$\cdot$	$\cdot$
$S_2$	$\cdot$	$\cdot$	$S_2 + X_{i-1}^2$	$S_2 + X_i^2$	$\cdot$	$\cdot$
$S_3$	$\cdot$	$\cdot$	$\cdot$	$S_3 + X_{i-1}^3$	$\cdot$	$\cdot$

**Figure 6.1:** Pipeline diagram to realize sum computation.

The most time consuming task is to compute these sums, since the higher order power of each signal sample is required in real-time. On the other hand, the further operations to compute the estimator  $k_3$  based on the sums, has to be done only once at the end of each measurement window.

The real-time computation of the sum terms was realized on the FPGA (hence there is no need to store the sampled signal values), and, after the transfer of the sums to the CPU of the Red-Pitaya board, the final operations to compute the cumulant estimator were performed by a control software running on the CPU.

Although the computation of the sums may seem trivial, the FPGA introduces two constraints, since it is not possible to use procedural programming at the hardware level. The constraints, which have to be taken into account are the following: first, only one operand can be used in an operation, and second, every operation in an algorithmic block is performed in parallel during a clock tick, and their results will be available at the end of the clock tick. For example, to compute the sum of the third order powers of the signal, one first needs to compute the second order power of the signal. This cannot be done in the same clock tick (for the operation  $x \cdot x \cdot x$ , the result of  $x \cdot x$  is needed, for which the result is not available immediately). Therefore, the computation of the powers and the sums have to be pipelined over several clock ticks. Fig. 6.1 illustrates the pipeline diagram of the computation of the sums.

A value measured by the ADC will be available for operations only in the following clock tick. Then, the FPGA is able to compute its square, and also the actual value of the first order sum can be evaluated. But the third power of the value and the second order sum can be computed only in the next clock tick. After the third power is available, the actual value of the third order sum can be computed during the following tick.

This introduces several inconveniences at the transfer of the sums, since they are not available at the same clock tick, but ideally the transfer should happen at the same time. By that time, the recording of the next time window (containing the next  $N$  samples) has to begin in order to sustain continuous operation. The solution to these issues and the implementation of the precise data transfer is detailed in Paper VII.

## 6.3 Implementation of the smart detector module

To realize the self-monitoring system, which was named as the smart detector module, the FPGA recorded the raw signal values provided by the ADC. The raw signal was transferred then to the CPU of the board, and the complex data processing, such as computing the PSD and determining its width, was done on the CPU.

This solution is relatively slow (due to the large amount of data transfer), but as it was shown in the previous chapter, the time is not crucial for self-monitoring.

## 6.4 Experimental results

After various laboratory tests of the device (detailed in Paper VII), a measurement campaign at the MINERVE reactor was dedicated to test the reliability of the measurement prototype. During the measurements, two different types of fission chambers were used: a CFUL01 chamber (considered as the reference chamber for the previous chapters), and a CFUR chamber, which is a smaller chamber and contains only  $10 \mu\text{g}$  uranium. For the sake consistency with the cases earlier discussed in this thesis, here only some results related to the CFUL01 chamber are highlighted.

### 6.4.1 Higher order Campbell results

During the measurement campaign, there was no opportunity to perform a transient measurement, hence the real time operation was tested at stationary power levels. Fig. 6.2 presents an example for the real time operation at 40 W reactor power. The third order cumulant was estimated at every 33 ms during almost a minute. The prototype performed well during the online measurement (the uncertainty of the estimation is due to the random errors, and the standard deviation of the mean of the estimated cumulant was less than 0.6 % with this time window).

In order to verify the linear behavior of the system, the third order cumulant has been estimated at reactor powers between 10 W and 80 W with the CFUL01, based on 33 ms time windows.

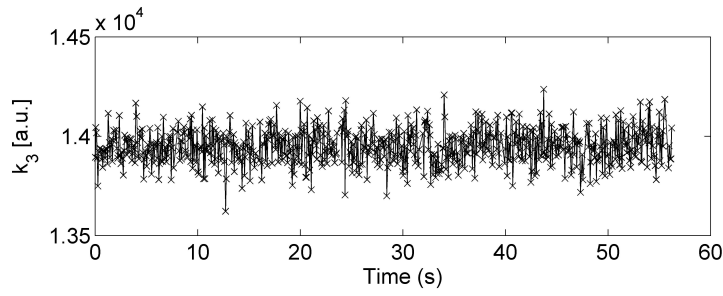


**Figure 6.2:** Real time cumulant measurement.

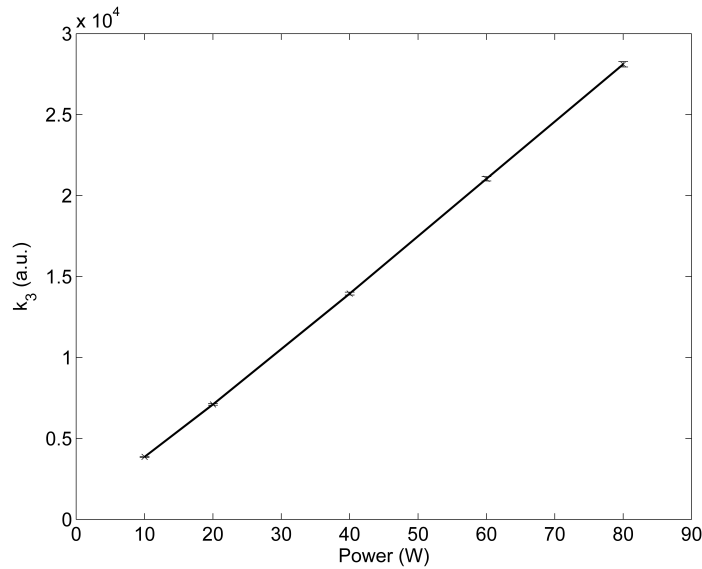


**Figure 6.3:** Cumulant estimation by the prototype device.

With the  $\pm 16$  V input range the whole power range of the reactor was covered. The obtained cumulant estimations are presented in Fig. 6.3. The measured third order cumulant shows linearity with the reactor power. The departure from linearity is lower than 1.6 %.

### 6.4.2 Smart detector results

The previous chapter investigated the PSD change due to the loss of filling gas pressure. The experimental investigation of the pressure loss requires a fission chamber with variable filling gas pressure or a fission chamber which is already malfunctioning. In our measurements neither of these were available. Therefore a variable parameter, which has similar impact on the pulse width, had to be identified.

As Fig. 6.4 shows (the plotted values are obtained by pyFC simulations), the increase in the voltage between the electrodes has a similar impact on the pulse

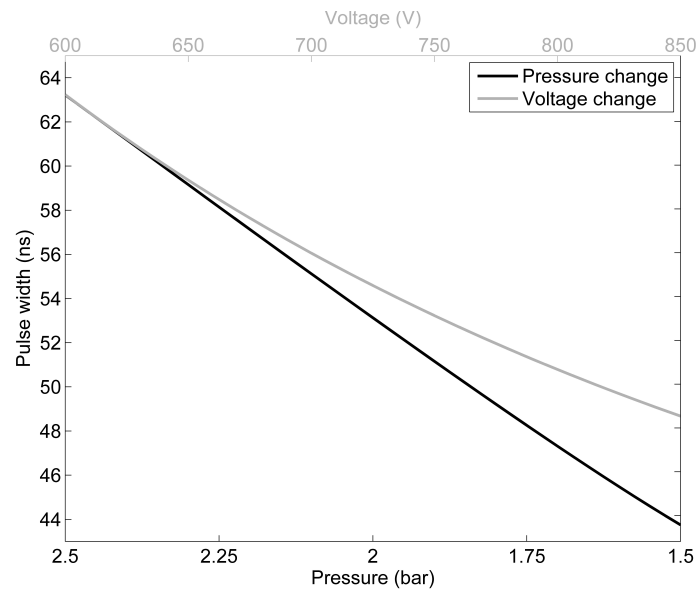


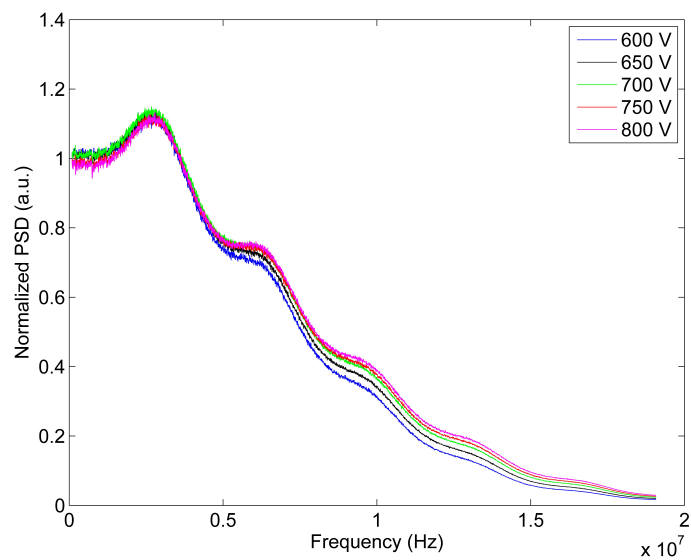
**Figure 6.4:** Simulated results of the pulse width vs the voltage and the gas pressure.

width as the decrease of the filling gas pressure. Since the voltage can be modified during the measurement, the PSD width was investigated at a constant reactor power of 20 W with the voltage changed between 600 V and 850 V (the CFUL01 chamber works in the saturation regime in this voltage range).

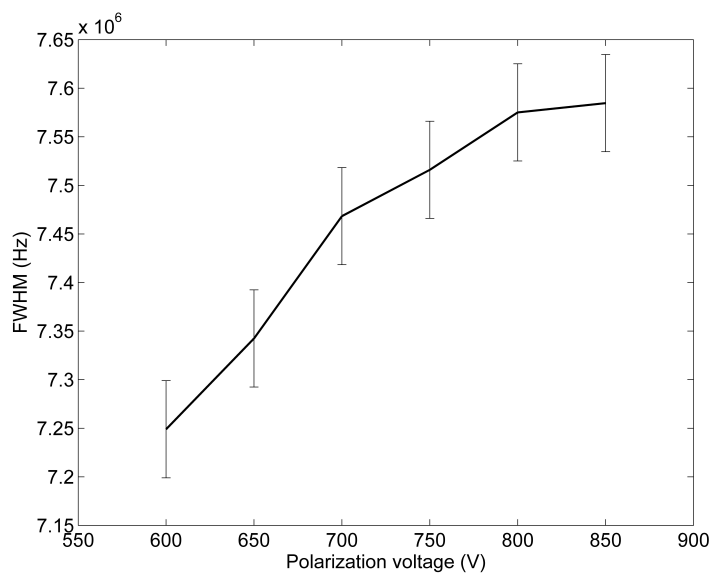
For each voltage, the PSD was calculated by averaging 4000 spectral densities of 0.52 ms long signals (i.e. the final PSD was based on a total measurement time of 2 seconds). With this signal length the uncertainty of the PSD already allowed to distinguish the change in the spectral width related to a change of 50 V. The measured PSD is shown in Fig. 6.5a, and the computed width is available in Fig. 6.5b. The small oscillation on the spectra is an artifact of the cable in the measurement.

Nevertheless, due to the slow data transfer between the FPGA and the CPU, the processing of this amount of data takes a few minutes (in this case the whole measured signal has to be transferred to the CPU). This means that the self-monitoring can be performed in every 2-3 minutes with the prototype.

The measurements with the prototype system proved the concept of the real-time self-monitoring capability based on the width of the PSD of fission chamber signals. However, by applying better performing devices, the time needed to measure the PSD width can be significantly reduced in the future.



(a) Measured PSD.



(b) Measured PSD width vs voltage.

**Figure 6.5:** Experimental results of the smart detector module.



## CHAPTER 7

### Concluding remarks

In this thesis three main areas were touched on: the limitations of the traditionally used fission chamber signal processing modes, the applicability of the higher order Campbell methods, and the self-monitoring capability of neutron monitoring systems. Here some of the conclusions are summarized, and also some further possible steps are mentioned.

- Concerning the traditional processing methods, sufficient overlap of the working regime of the pulse and Campbelling mode requires short pulse length. This could be achieved by increasing the nitrogen content in the filling gas. However, the nitrogen molecules disappear under irradiation at high temperature. Therefore, for applications such as Sodium cooled Fast Reactors, the development of the processing method is favored instead of changing the chamber design.
- By applying higher order Campbelling methods, it is possible to suppress the impact of the noise, the gamma (from the reactor) and the alpha (from the fissile deposit) background radiation. These methods provide an accurate count rate estimation at a wide count rate range. Nevertheless, the random uncertainties increase with the order of the method, and at really high count rates (above  $10^9 \text{ s}^{-1}$ ) the random errors tend to overcome the benefits of the method. Hence, the application of higher than third order methods is not feasible, nonetheless the even higher order methods do not provide significant advantages. With the use of third order mode, the real-time measurement can be based on a few ms long samples, which is sufficient to achieve real time monitoring. It was shown that the third order mode may work even at really low count rates (such as  $10^3 \text{ s}^{-1}$ ), but for that it requires a measurement length of a few seconds (nevertheless, the traditional pulse mode has the same drawback).
- The experimental calibration of the third order method is possible through investigating the pulse shape and the amplitude distribution of the pulses, therefore the count rate of the fission chamber signal can be estimated. But, at the moment the calibration is done off-line (by post-processing the recorded signal). This may be problematic, since the system measuring the third order cumulant is not necessarily capable of recording the signal. Therefore

the signal recording may be done with a separate system, which can have a different transfer function. A possible way to overcome this issue is to perform an empirical calibration, where the count rate is estimated with pulse counting techniques and compared to the measured cumulant. Such a calibration would not be plausible for the traditional Campbell method, due to the linearity gap between the pulse counting methods and the second order Campbell.

- In case the fission chamber is malfunctioning (for example the filling gas leaks through a crack), it is possible to detect this change from the PSD of the fission chamber signal. In order to achieve a low uncertainty on the spectral width measurements, a few seconds long samples are needed. Nevertheless, the estimated characteristic time for a filling gas pressure loss is in the order of magnitude of minutes, hence the early detection of malfunction is possible.
- Based on FPGAs the implementation of the third order Campbell mode for real time application is feasible. Using a relatively simple electronics device, which features an ADC, a CPU and an FPGA on board, a prototype measurement system was built and tested. The device proved the reliability and robustness of the concept. However, for the future industrial use, a better performing board may be favorable. It has to be highlighted again that the main drawback of the third order Campbell mode and of the device is the relatively challenging calibration. In order to perform the calibration, the developed device was capable to record the raw signal, which increased the complexity of the implementation. The calibration had to be done in the post-processing phase. As a further step an automatic, online calibration procedure is under development.
- Since the cumulant estimation was realized by pipelining the measured data through several clock cycles, the data transfer between the FPGA and the CPU is fast. On the contrary, for the self-monitoring module the device had to transfer larger amount of data between the FPGA and the CPU, therefore the PSD width measurement was possible only in every few minutes. This is already a remarkable achievement in regular monitoring, but with the use of higher performance devices in the future, this time can be significantly reduced.
- Fission chambers have some technological uncertainties (the size of the electrodes, the applied voltage, the nitrogen content of the filling gas, etc.). In the future, the impact of these uncertainties on the current pulses generated in the fission chamber will be investigated with the pyFC tool.

---

## Acknowledgements

First of all I would like to thank my supervisor, Professor Imre Pázsit for his endless mentoring, tutoring and support both in academic life and in life. He has an unbelievable knowledge about everything (stochastic processes, reactors, paprika growing, and even ulti!). Örök hálám.

My supervisors at CEA, Christian and Philippe. I received an incredible amount of help. Merci! From Philippe, I had the opportunity to learn about every possible details of fission chambers, pulses and simulations, but we had hilarious discussions about the dark side as well (of course I mean the SW universe). May the force be with you, Master!

Special thanks to Lénárd Pál, with whom I had the opportunity to work together for a short while. Meeting and "meditating about the stochastic signals" with him was one of the most memorable moments of this PhD period.

My present and former officemates during these four years, I am extremely lucky since you were so many and also because all of you are more easygoing than me. It was a great pleasure to share place and time with you inside and outside work: Florian, Micke, Fredrik, Manu, Vasu, Greg, Vlad, Klara and Alberto. With Greg, I even had the opportunity to work on some topics together, his knowledge on signal processing, programming, counting spectra and abusing English is fascinating, it was awesome to brainstorm with him so many times. I also would like to mention the other youngsters from Nephy, with whom I had the pleasure to share some fika, beers and conversations about life: Augi, Sebas and Victor. Thanks a lot guys, best times ever!

All my colleagues at Nephy, thank you so much for the great times, conversations and the infinite help: Anders' sense of humor was a real spice during fika in this spiceless Sweden. Lennart and Lasse are for sure the bests when it comes to computers. It was great to have Christophe and Paulo in this collaboration, their pragmatic views on how science works (or should work) was eye-opening. And Jóska is such a real Hungarian, he helped me a lot not to feel homesick.

Merci à tous mes collègues du LDCI. J'ai eu beaucoup des souvenirs inoubliables et aussi beaucoup de vins. Remerciement spécial pour Christelle, qui est très amiable et "chatty", et Jean-Michel, mon ami, qui a cru que je serai capable d'apprendre le français (et avec son aide, j'y suis un peu parvenu).

Great thanks for the Swedish Research Council for the financial support and the ESNII+ project for letting me participate on some of their workshops.

Thank you, my SG friends and other Hungarian physicist friends to always feel myself welcomed in Hungary, sharing some traveling experience and for visiting me occasionally.

But most importantly, there are probably not enough words. My family: Anya, Apa, Csabi, Niki and Zsuzsi and your family: Köszönök mindent!

---

## BIBLIOGRAPHY

- [1] Richard G. Hewlett and Oscar E. Anderson. *The New World, 1939-1946*. University Park: Pennsylvania State University Press, 1962.
- [2] S. Normand. "Instrumentation Nucleaire pour les systemes industriels de mesure". Habilitation. Université de Caen, 2010.
- [3] F. Gauché. "Generation IV reactors and the ASTRID prototype: Lessons from the Fukushima accident". In: *Comptes Rendus Physique* 13 (2012), pp. 365–371.
- [4] C. Jammes, P. Filliatre, B. Geslot, T. Domenech, and S. Normand. "Assessment of the high temperature fission chamber technology for the French fast reactor program". In: *IEEE Transactions on Nuclear Science* 59 (2012), pp. 1351–1359.
- [5] M. A. Reichenberger, P. B. Ugorowski, J. A. Roberts, and D. S. McGregor. "First-order numerical optimization of fission-chamber coatings using natural uranium and thorium". In: *2014 IEEE Nuclear Science Symposium and Medical Imaging Conference (NSS/MIC)*. 2014.
- [6] B. Lescop et al. "A new system for in-core wide range neutron monitoring". In: *Nuclear Science Symposium Conference Record, 2004 IEEE*. Vol. 3. 2004, pp. 1567–1570.
- [7] G. F. Knoll. *Radiation Detection and Measurement*. 4th. John Wiley & Sons, 2010.
- [8] P. Filliatre, C. Jammes, B. Geslot, and L. Buiron. "In vessel neutron instrumentation for sodium-cooled fast reactors: Type, lifetime and location". In: *Annals of Nuclear Energy* 37 (2010), pp. 1435–1442.
- [9] Chang. J. *Table of Nuclides, KAERI(Korea Atomic Energy Research Institute)*. <http://atom.kaeri.re.kr/>. Accessed: 2016. August. 2016.
- [10] P. Filliatre, L. Oriol, C. Jammes, and L. Vermeeren. "Joint estimation of the fast and thermal components of a high neutron flux with a two on-line detector system". In: *Nuclear Instruments and Methods in Physics Research Section A: Accelerators, Spectrometers, Detectors and Associated Equipment* 603 (2009), pp. 415–420.
- [11] B. Geslot et al. "New measurement system for on line in core high-energy neutron flux monitoring in materials testing reactor conditions". In: *Review of Scientific Instruments* 82 (2011).

- [12] T. E. Bortner, G. S. Hurst, and W. G. Stone. "Drift velocities of electrons in some commonly used counting gases". In: *Rev. Sci. Instrum.* 28 (1957), pp. 103–108.
- [13] G. N. Haddad. "Drift Velocity of Electrons in Nitrogen-Argon Mixtures". In: *Aust. J. Phys.* 36 (1983), pp. 297–303.
- [14] G. J. M. Hagelaar and L. C. Pitchford. "Solving the Boltzmann equation to obtain electron transport coefficients and rate coefficients for fluid models". In: *Plasma Sources Sci. Technol.* 14 (2005), pp. 722–733.
- [15] S.F. Biagi. "Monte Carlo simulation of electron drift and diffusion in counting gases under the influence of electric and magnetic fields". In: *Nuclear Instruments & Methods in Physics Research, Section A: Accelerators, Spectrometers, Detectors, and Associated Equipment* 421 (1999), pp. 234–240.
- [16] P. Filliatre, C. Jammes, B. Geslot, and R. Veenhof. "A Monte Carlo simulation of the fission chambers neutron-induced pulse shape using the GARFIELD suite". In: *Nuclear Instruments and Methods in Physics Research Section A: Accelerators, Spectrometers, Detectors and Associated Equipment* 678 (2012), pp. 139–147.
- [17] C. Jammes, P. Filliatre, P. Loiseau, and B. Geslot. "On the impact of the fissile coating on the fission chamber signal". In: *Nuclear Instruments and Methods in Physics Research Section A: Accelerators, Spectrometers, Detectors and Associated Equipment* 681 (2012), pp. 101–109.
- [18] N. R. Campbell and V. J. Francis. "A Theory of Valve and Circuit Noise". In: *JIEE* 93 (1946), pp. 45–52.
- [19] R. A. DuBridge. "Campbell Theorem - System Concepts and Results". In: *IEEE Transactions on Nuclear Science* 14 (1967), pp. 241–246.
- [20] I. Lux and A. Baranyai. "Higher order campbell techniques for neutron flux measurement: I. Theory". In: *Nuclear Instruments and Methods in Physics Research* 202 (1982), pp. 469–475.
- [21] B. Bärs. "Variance and higher order signal moments in neutron flux measurements". In: *Nuclear Instruments and Methods in Physics Research Section A: Accelerators, Spectrometers, Detectors and Associated Equipment* 275 (1989), pp. 403–410.
- [22] R. A. Fisher. "Moments and Product Moments of Sampling Distributions". In: *Proceedings of the London Mathematical Society* 33 (1928), pp. 199–238.
- [23] P. Loiseau, B. Geslot, and J. Andre. "On the fission chamber pulse charge acquisition and interpretation at MINERVE". In: *Nuclear Instruments and Methods in Physics Research Section A: Accelerators, Spectrometers, Detectors and Associated Equipment* 707 (2013), pp. 58–63.
- [24] E. W. Pontes and A. Ferreira. "Using cumulants and spectra to model nuclear radiation detectors". In: *IEEE Transactions on Nuclear Science* 53 (2006), pp. 1292–1298.

- 
- [25] J. F. Ziegler, J. P. Biersack, and M. D. Ziegler. *The Stopping and Range of Ions in Matter*. 2008. URL: [srim.org](http://srim.org).
- [26] W. Shockley. "Currents to Conductors Induced by a Moving Point Charge". In: *Journal of Applied Physics* 9 (1938), pp. 635–636.
- [27] Zs. Elter. *pyFC: a TRIM-based fission chamber pulse shape simulator*. Tech. rep. CTH-NT-318. Chalmers University of Technology, 2015.
- [28] S. N. Ahmed. *Physics and Engineering of Radiation Detection*. Academic Press, 2007.
- [29] A. Gruel, P. Leconte, D. Bernard, P. Archier, and G. Noguère. "Interpretation of Fission Product Oscillations in the MINERVE Reactor, from Thermal to Epithermal Spectra". In: *Nuclear Science and Engineering* 169 (2011), pp. 229–244.
- [30] *CFUL01 data sheet*. <https://www.photonis.com/uploads/datasheet/ngd/CFUL01.pdf>. Accessed: 2016. August.
- [31] T. Rivero Gutiérrez, J. S. Benítez-Read, J. C. Palacios Hernández, A. Segovia-de-los-Ríos, and L. C. Longoria-Gándara. "Software-based Neutron Flux Measurement Channel (NFMC)". In: *Int. J. Nuclear Energy Science and Technology* 5 (2010), pp. 91–104.
- [32] V. Bécares and J. Blázquez. "Detector Dead Time Determination and Optimal Counting Rate for a Detector Near a Spallation Source or a Subcritical Multiplying System". In: *Science and Technology of Nuclear Installations 2012* (2012).
- [33] M. A. Schultz. *Control of nuclear reactors and power plants*. McGraw-Hill, 1955.
- [34] L. Vermeeren et al. "Experimental Verification of the Fission Chamber Gamma Signal Suppression by the Campbelling Mode". In: *IEEE Transactions on Nuclear Science* 58 (2011), pp. 362–369.
- [35] C. Dubi et al. "Dead Time Corrections using the Backward Extrapolation Technique". In: *Physor conference*. 2016.
- [36] C.T.I.I. Norman. "Gamma and alpha compensated fission chamber". US Patent 4,071,764. Jan. 1978. URL: <https://www.google.com/patents/US4071764>.
- [37] B. Geslot et al. "Method to Calibrate Fission Chambers in Campbelling Mode". In: *IEEE Transactions on Nuclear Science* 59 (2012), pp. 1377–1381.
- [38] I. Lux and A. Baranyai. "Higher order campbell techniques for neutron flux measurement: II. Correlated Campbelling". In: *Nuclear Instruments and Methods in Physics Research* 202 (1982), pp. 477–480.
- [39] L. B. Baers, T. Rivero Gutierrez, R. A. Carrillo Mendoza, and Jimenez Santana G. "Use of Higher Order Signal Moments and High Speed Digital Sampling Technique for Neutron Flux Measurements". In: *IEEE Transactions on Nuclear Science* 40 (1993), pp. 832–839.

- [40] E. W. Weisstein. *k-Statistic - From MathWorld—A Wolfram Web Resource*. <http://mathworld.wolfram.com/k-Statistic.html>. Accessed: 2016. August. 2016.
- [41] P. Filliatre, L. Vermeeren, C. Jammes, B. Geslot, and D. Fourmentel. “Estimating the  $\gamma$ -ray contribution to the signal of fission chambers with Monte Carlo simulations”. In: *Nuclear Instruments and Methods in Physics Research Section A: Accelerators, Spectrometers, Detectors and Associated Equipment* 648 (2011), pp. 228–237.
- [42] L. Pál and Pázsit. “Campbell-type theory of fission chamber signals generated by neutron chains in a multiplying medium”. In: *Nuclear Instruments and Methods in Physics Research Section A: Accelerators, Spectrometers, Detectors and Associated Equipment* 794 (2015), pp. 90–101.
- [43] R. Hunt. “Testing Fission Chambers”. In: *Nuclear Engineering International magazine* (2011). URL: <http://www.neimagazine.com/features/featuretesting-fission-chambers/>.
- [44] M. Thevenin et al. “Digital Real-Time Multiple Channel Multiple Mode Neutron Flux Estimation on FPGA-based Device”. In: *EPJ Web of Conferences* 106 (2016).
- [45] *Red-Pitaya homepage*. <http://redpitaya.com/>. Accessed: 2016. August.

Papers I-VII

